

**Oiling-out Crystallization on Solid Surfaces Controlled by Solvent  
Exchange**

by

Howon Choi

A thesis submitted in partial fulfillment of the requirements for the degree of

Master of Science

in

Chemical Engineering

Department of Chemical and Material Engineering  
University of Alberta

© Howon Choi, 2021

# Abstract

Oiling-out, also termed as liquid-liquid separation (LLPS), is a phenomenon well observed in cooling crystallization when the solution becomes cloudy due to a second liquid phase formation. One way to control LLPS is solvent exchange, where surface droplets are produced in the bottom-up approach. In this process, a good solvent for oil is displaced by a poor solvent, leading to oil droplet nucleation and subsequent growth. The droplets were immobilized on the surface; therefore, dynamics of the droplet formation and growth from LLPS can be monitored with time and quantitatively studied.

In this work, the oiling-out of a model component (beta-alanine) in the mixture of isopropanol and water was investigated. The aqueous solution was displaced by isopropanol in a microchamber at controlled flow conditions. The solute-rich droplets were followed on the various substrates during the process of oiling-out. The changes in parameters such as flow rate and channel height affected the transfer of solvents, and different crystal morphology was observed. Usage of heterogeneous surfaces led

to the confinement of droplets and the formation of a thin film with micro-holes or a connected network of crystals. Rough micro-structures on the surface allowed the easy detachment of crystals from the surface. The solvent exchange crystallization can form crystals at a very low concentration of the solute, and the crystals can be used as seeds to trigger crystallization in bulk solution. Beyond oiling-out crystallization, the results demonstrated that the crystal formation from another solute dissolved in the droplets could be triggered by solvent exchange. The length of crystal fibers after the solvent exchange process was shorter at a faster flow rate. This work suggested that the solvent exchange has the potential to be an effective approach for controlling oiling-out crystallization, which can be applied in the separation and purification of many food, medical, and therapeutic ingredients.

# Preface

This thesis is an original work by me, Howon Choi. The literature review in Chapter 2 and concluding analysis in Chapter 6 are my original work. The method and procedure in Chapter 3 were written with the assistance of Jae Bem You on the procedure for chemically patterning a substrate and Zixiang Wei on the solution preparation and edits in the substrate preparation.

Chapter 4 of this thesis is a modified version of the journal article that has been published as “Oiling-out Crystallization of Beta-alanine on Solid Surfaces Controlled by Solvent Exchange” in *Advanced Materials Interfaces*. I was an equal contributor as the second author of the work and was responsible for part of oiling-out crystallization data collection and analysis. The published work was written and supervised by Xuehua Zhang. Zixiang Wei collected most of the data presented in the paper. Hao Hao provided the data analysis program for crystal growth. Huaiyu Yang helped with data interpretation and manuscript edits. Chapter 4 is based on the previous iteration of the manuscript, which I came up as an initial draft but was discontinued from excessive leave due to the COVID. Chapter 5 of this thesis has been submitted as “Effects of Chemical and Geometric Micro-structures on Oiling-out Crystallization by Using Solvent Exchange”. I am the main contributor, and I am responsible for data collection and analysis, as well as drafting the initial version of the manuscript. Jae Bem You provided the patterned substrates for the experiments. Zixiang Wei prepared micro-lens substrate and Huaiyu Yang assisted in the manuscript editing. Xuehua Zhang was the supervisory author and revised the manuscript.

# Acknowledgements

First, I would like to thank my supervisor, Dr. Xuehua Zhang, for her nurturing guidance and excellent support during my graduate studies. Her outstanding mentorship led me to great opportunities to learn various equipment and techniques that would have otherwise been unreachable. Even during struggling times, her support and advice pushed me to continue on with the projects. In many cases, I have felt her patience as I slowly understood the subject and improved upon the skills I lacked. Truly, this thesis would have never come to fruition without her help.

The project is supported by the Natural Science and Engineering Research Council of Canada (NSERC) and Future Energy Systems (Canada First Research Excellence Fund). This research was undertaken, in part, thanks to funding from the Canada Research Chairs program. I am grateful for their financial support, which helped me through my two years in completing my graduate degree.

I thank Zixiang Wei for the valuable discussion on oiling-out crystallization and providing some experimental data for me. He has been a great example to follow and I have learned many laboratory skills under his helps. I thank Dr. Mark Hao in Swinburne University, Australia for providing the crystal growth analysis by his coding. I thank Dr. Jae Bem You for helping me with providing patterned substrates and many discussions/feedback about the project while in his busy schedule. I thank I thank Dr. Al Meldrum in Department of Physics, University of Alberta and Dr. Sergey Vagin in Department of Chemistry, University of Munich, Germany for generously supplying us with materials for one of our experiments. I also want to thank all the soft matter and interface research group members that I am so proudly a part

of and the countless times they gave me supports and helps.

I also would like to thank my family members for their loving support and counseling throughout the years. It comforted me when I saw them during the holidays and helped me take my mind off of stressful moments. I also want to express my gratitude for my friends who also helped me through graduate school, as their conversations and activities would cheer me up from time to time.

Once again, I thank everyone I have mentioned above and all those I have met during my studies. I hope that all will be happy in their future endeavors.

# Table of Contents

<b>1</b>	<b>Introduction</b>	<b>1</b>
1.1	Background . . . . .	1
1.2	Motivation . . . . .	2
1.3	Thesis objectives . . . . .	3
1.4	Thesis outline . . . . .	3
<b>2</b>	<b>Literature review</b>	<b>5</b>
2.1	Solvent exchange . . . . .	5
2.1.1	Introduction . . . . .	5
2.1.2	Liquid-liquid phase separation (LLPS) . . . . .	6
2.1.3	Parameters for controlling the solvent exchange . . . . .	7
2.1.4	Growth and dissolution dynamics of droplets . . . . .	11
2.2	Techniques used in the literature for surface droplet measurement . . . . .	17
2.3	Crystallization of classical nucleation and oiling-out phenomenon . . . . .	18
2.3.1	Introduction . . . . .	18
2.3.2	Common types of crystallization . . . . .	19
2.3.3	Crystalline structure and equipment for crystal studies . . . . .	20
2.3.4	Classical nucleation theory (CNT) . . . . .	22
2.3.5	Heterogenous nucleation on solid surface . . . . .	23
2.3.6	Oiling-out crystallization . . . . .	24
2.3.7	Two-step nucleation theory . . . . .	25
2.3.8	Counter diffusion of oiling-out droplet crystallization . . . . .	28

2.4	Conclusions . . . . .	29
2.5	Knowledge gaps in research on oiling-out crystallization . . . . .	30
<b>3</b>	<b>Methods and procedure</b>	<b>31</b>
3.1	Substrate preparation . . . . .	31
3.2	Solution preparation . . . . .	33
3.3	Procedure of oiling-out crystallization by solvent exchange . . . . .	33
3.4	Conditions for solvent exchange: solute concentration, flow rate, and channel height . . . . .	34
3.5	Crystallization in bulk mixture triggered by seeds . . . . .	36
3.6	Data collection and image analysis . . . . .	36
3.7	Chemical and structural identification . . . . .	37
<b>4</b>	<b>Oiling-out crystallization of beta-alanine on homogeneous surfaces controlled by solvent exchange</b>	<b>38</b>
4.1	Results and discussion . . . . .	38
4.1.1	General trends for oiling-out crystallization through solvent ex- change . . . . .	38
4.1.2	Liquid-liquid phase separation by solvent exchange and droplet characterization . . . . .	39
4.1.3	Crystallization: morphology and characterization . . . . .	44
4.1.4	Effect of surface wettability . . . . .	49
4.1.5	Discussion . . . . .	51
4.1.6	Solution crystallization in liquid-liquid phase separated solution triggered by the seed crystals . . . . .	53
4.2	Conclusion . . . . .	55
<b>5</b>	<b>Effects of chemical and geometric micro-structures on crystallization of surface droplets during solvent exchange</b>	<b>57</b>

5.1	Results and discussion . . . . .	57
5.1.1	Oiling-out crystallization on surfaces with chemical micro-patterns	57
5.1.2	Oiling-out crystallization on micro-structured surfaces . . . . .	66
5.1.3	Fiber crystal formation from droplets without oiling-out . . . . .	68
5.2	Conclusion . . . . .	70
<b>6</b>	<b>Conclusions, recommendations, &amp; future work</b>	<b>72</b>
6.1	Conclusions . . . . .	72
6.2	Future work . . . . .	73
	<b>Bibliography</b>	<b>75</b>
	<b>Appendix A:</b>	<b>84</b>
A.1	Section 1 . . . . .	84

# List of Tables

2.1	List of techniques to observe surface droplets . . . . .	18
2.2	List of techniques for observing crystallization and crystal products .	21
2.3	Example substances with oiling-out crystallization behaviour from the literature . . . . .	26
3.1	List of experimental conditions on homogeneous surfaces (Chapter 4)	35
3.2	List of experimental conditions on micro-patterned surfaces (Chapter 5)	35

# List of Figures

2.1	Phase diagram with one-phase and two-phase regimes . . . . .	7
2.2	Effect of initial concentration on droplet formation through solvent exchange . . . . .	9
2.3	Surface droplet morphology . . . . .	12
2.4	Droplet dissolution/growth modes . . . . .	14
2.5	The flow profile and oversaturation level during solvent exchange . . .	15
2.6	The flow profile and oversaturation pulse shift due to gravity during solvent exchange . . . . .	17
2.7	The relation of interfacial energy, bulk energy, and the total free energy in classical nucleation theory (CNT) . . . . .	23
2.8	Heterogeneous nucleation and the relation to surface contact angle . .	24
2.9	Schematic diagrams of the free energy of CNT and the two-step nucleation theory . . . . .	27
2.10	Schematic diagrams of the two-step nucleation theory . . . . .	28
2.11	Diagrams of spherical crystallization process by quasi-emulsion solvent diffusion (QESD) method . . . . .	29
3.1	Solvent exchange process and ternary phase diagram . . . . .	34
4.1	Progression of oiling-out crystallization on $SiO_2$ substrate . . . . .	39
4.2	Plot of supersaturation acquired from droplet growth . . . . .	41
4.3	Plot of probability distribution function of droplet radius with varying flow rate . . . . .	42

4.4	Snapshots of three separate runs of oiling-out crystallization with varying flow rates . . . . .	43
4.5	Optical microscopy of droplet crystallization triggered by droplets . .	45
4.6	Diagram of thin film crystal growth by droplet coalescence and without coalescence . . . . .	46
4.7	Optical microscopy of droplet crystallization of different crystal morphology caused by facet effect . . . . .	47
4.8	Snapshots and plots for crystal growth analysis for oiling-out crystallization . . . . .	48
4.9	Graphic description of oiling-out crystallization on different substrates	49
4.10	Images of oiling-out crystallization on different substrates . . . . .	50
4.11	FTIR and XRD data of alanine crystals . . . . .	51
4.12	Crystallization in LLPS droplet . . . . .	52
4.13	Oiling-out crystallization for lower concentration . . . . .	53
4.14	Crystal seed experiment in bulk solution . . . . .	54
5.1	Oiling-out crystallization on the hydrophobic patterned substrate . .	58
5.2	Oiling-out crystallization on the hydrophilic patterned substrates. . .	59
5.3	Oiling-out crystallization of droplets on homogeneous vs patterned substrates . . . . .	60
5.4	Oiling-out crystallization with a low alanine concentration . . . . .	60
5.5	Oiling-out crystallization at different flow rate . . . . .	61
5.6	Reproducibility of oiling-out crystallization . . . . .	62
5.7	Decreasing droplet size with decrease in channel heights . . . . .	64
5.8	Oiling-out crystallization on the lens array . . . . .	66
5.9	Oiling-out and crystallization induced by a bubble . . . . .	67
5.10	Ternary phase of mesitylene, ethanol, and water and a diagram of fiber formation in surface droplet . . . . .	68

5.11	Fiber formation in droplet on OTS substrate through solvent exchange	69
A.1	Plot of droplet size distribution on $SiO_2$ with varying flow rates . . .	84

# List of Symbols

$A$	Exponential prefactor	$N/m$
$Ar$	Archimedes number	
$G$	Gibbs free energy	$J$
$H$	Height of a surface droplet	$\mu m$
$J$	Rate of nucleation	$/s$
$L$	Lateral diameter of a surface droplet	$nm$
$M$	Mass of the solute	$mg$
$Pe$	Peclet number	
$Q$	Volumetric flow rate	$mL/hr$
$R$	Radius of the droplet	$\mu m$
$T$	Temperature	$K$
$V$	Volume of the droplet	$mL$
$\Delta G$	Total Gibbs free energy	$J$
$\Delta G'_c$	Total Gibbs free energy at critical radius for heterogeneous nucleation	$J$
$\Delta G_{L-L}$	Formation free energy of the intermediate liquid phase	$J$
$\Delta G_c$	Total Gibbs free energy at critical radius	$J$
$\Delta\rho$	Difference in density	$g/mL$

$\bar{U}$	Average flow velocity	$m/s$
$c_\infty$	Concentration of solute in the bulk flow	$g/mL$
$c_{sat,good}$	Saturation concentration of solute in the good solvent	$g/mL$
$c_{sat,poor}$	Saturation concentration of solute in the poor solvent	$g/mL$
$c_s$	Concentration of solute at the interface	$g/mL$
$h$	Channel height of the flow cell	$\mu m$
$r_c$	Critical radius	$nm$
$t$	Time	$s$
$t_0$	Initial time	$s$
$w$	Channel width of the flow cell	$\mu m$

### Constants

$D$	Diffusion constant	$m^2/s$
$k_b$	Boltzmann constant	$1.38 \times 10^{-23} J/K$

### Greek

$\gamma$	Interfacial tension	$N/m$
$\mu$	Dynamic viscosity	$Pa \cdot s$
$\nu$	Kinematic viscosity	$m^2/s$
$\phi$	Numerical factor related to heterogeneous nucleation	
$\rho$	Density of the phase	$g/mL$
$\sigma$	Surface tension	$N/m$
$\theta$	Contact angle of a surface droplet	

# Abbreviations

**AFM** Atomic force microscopy.

**API** Active pharmaceutical ingredient.

**APTES** 3-Aminopropyltriethoxysilane.

**ATR** Attenuated total internal reflection.

**CA mode** Constant contact angle mode.

**CNT** Classical nucleation theory.

**CR mode** Constant radius mode.

**DHDPS** 4,4' dihydroxydiphenylsulfone.

**DSC** Differential scanning calorimetry.

**FBRM** Focused beam reflectance measurement.

**FTIR** Fourier transform infrared spectrum.

**HDODA** 1, 6-hexanediol diacrylate.

**IPA** Isopropanol.

**L-L** Liquid-liquid.

**LLPS** Liquid-liquid phase separation.

**Np-P4VB** 2,5-Bis(2-(4-pyridyl)-vinylene) hydroquinone dineopentyl ether.

**OTS** octadecyltrichlorosilane.

**PAT** Process analytical technologies.

**PEGDME** Polyethyleneglycoldimethylether.

**PVM** Particle video microscope.

**QCM** Quartz crystal microbalance.

**QESD** Quasi-emulsion solvent diffusion.

**RIE** Reactive ion etching.

**S-L-L** Solid-liquid-liquid.

**S-L** Solid-liquid.

**STP** Standard room temperature and pressure.

**TEM** Transmission electronic microscopy.

**THF** Tetrahydrofuran.

**TIRF** Total internal reflection fluorescence.

**UV** Ultraviolet light.

**Vis** Visible light.

**XRD** X-ray diffraction.

# Chapter 1

## Introduction

### 1.1 Background

Oiling-out crystallization[1, 2] is a phenomenon where a secondary liquid phase is formed preceding the crystallization[3]. This phenomenon is often observed in many proteins, polymers, active pharmaceutical ingredients (Ibuprofen, erythromycin ethylsuccinate, idebenone, and butyl paraben) and other chemicals (Vanillin and lauric acid)[1, 4–13]. After oiling-out, the solution with agitation becomes cloudy due to the formation of droplets (dispersed phase) in the continuous phase but eventually separates into two layers of subphases. Oiling-out often creates negative consequences during the crystallization process. The impurities tend to be more soluble in the secondary liquid phase created by oiling-out. Therefore, the crystal product purity may be affected, or the new phase may cause higher energy demand for chemical mixing due to adsorption to the equipment[14]. Many studies have tried to avoid this phenomenon by lowering the initial concentration, adjusting temperature and pressure, seeding, and employing ultrasounds[15–18]. On the other hand, some studies show that the oiling-out crystallization can be controlled to achieve different crystal sizes[5], shapes (spherical[19–21], porous[22], or other[23, 24]), and can even control enantiomeric separation[4], and polymorphism[25].

For crystallization, the supersaturation and how it is achieved is essential to the process. While the majority of studies have focused on controlling droplet forma-

tion, we have demonstrated that different crystallization can be achieved through the solvent exchange method by adjusting the flow rate[26]. The solvent exchange obtains this supersaturation by replacing good solvent (high solute solubility) with poor solvent (low solute solubility)[27]. The solvents are miscible, while the solute is only miscible in a good solvent, leading to droplet nucleation. In this thesis, the solution would experience droplet formation and crystallization through the process of oiling-out crystallization. Starting from a homogeneous solution, the concentration change would lead to liquid-liquid phase region, then to metastable liquid-liquid-solid phase region, to finally end with liquid-solid phase region where the final product can be collected after air-drying.

The solvent exchange method allows individual droplets to be observed with time. As the droplet morphology and crystallization is observe via an optical microscope, the dynamics of nucleation of oiling-out crystals in the surface droplets can be studied. Further investigation has shown that liquid-liquid separation behaviour on different substrates may be controlled by optimizing simple parameters such as flow rate, initial concentrations, and channel heights. Through this study, we hope to further understand and control the crystallization from droplets in order to integrate with the application of pharmaceutical production and other future implementations.

## 1.2 Motivation

Regarding the chemicals that exhibit oiling-out during the crystallization process, we believed that the solvent exchange method would be a useful way to control the phenomenon. Parameters such as initial concentration ratio, the flow rate of solution B (antisolvent), surface property, and channel height have shown to be an effective way to control the LLPS for oil droplet formation through solvent exchange method. Therefore, the same parameters were tested for the oiling-out crystallization processes. With the chosen compound of beta-alanine, which exhibited oiling-out crystallization in standard room temperature and pressure, the progress of how the

droplet formed and crystallized was observed through an optical microscope. The experiments showed significant differences with varying substrates and patterned substrates with different wettability. This work also demonstrates that the oiling-out crystallization from droplets with solvent exchange is a potential method to screen and explore the new morphology of the crystalline product.

### **1.3 Thesis objectives**

The main objectives of this study area are as following:

1. to incorporate solvent exchange method with oiling-out crystallization with the model solution of beta-alanine, water, and isopropanol mixture.
2. to adjust the parameters (such as flow rate, initial concentration, channel height, and surface properties) with solvent exchange to observe the effects of the oiling-out process and the crystallization process.
3. to test different chemicals that exhibit crystallization in surface droplets and find the validity of the solvent exchange method for broader applications.
4. to examine the effect of using different substrates (including a patterned substrate with heterogeneous wettability) on the oiling-out crystallization and its viability in controlling the oiling-out crystallization.
5. to explain the behaviours of oiling-out crystallization seen in the solvent exchange experiments with theories from the literature.

### **1.4 Thesis outline**

In Chapter 1, the motivation for the work, objectives for the thesis, and the thesis outline, along with the lists of figures and tables, will be introduced. In Chapter 2, the literature about the solvent exchange will be reviewed along with the theory

behind the mechanism of liquid-liquid separation during the solvent exchange. Then the literature on crystallization and the phenomenon of oiling-out crystallization will be reviewed. In Chapter 3, the method, procedure, and equipment used for the experiments in Chapters 4 and 5 will be discussed. In Chapters 4 and 5, experimental results for oiling-out crystallization using solvent exchange will be discussed along with the explanation of the observed phenomenon. Chapter 6 will summarize the two works discussed in Chapters 4 and 5, and end with possible future works on the usage of solvent exchange flow cells to control oiling-out crystallization.

# Chapter 2

## Literature review

### 2.1 Solvent exchange

#### 2.1.1 Introduction

Solvent exchange is a simple protocol to induce surface nanodroplets[28–34]. Surface droplets are a liquid phase on a surface in contact with the surrounding medium[30, 35]. Typically, the stability of the droplet depend on their solubility in the immiscible solvent[29, 36]. Solvent exchange can produce surface nanodroplets with a long lifetime[28]. Solvent exchange also showed improvement in reproducibility, which along with improved lifetime, would benefit in utilizing the droplets for different applications[28, 37–40]. These droplets are currently being researched in lubrication, biosensors, chemical analysis, lab-on-chip devices, and others as the nanoscale nature of the droplets has higher efficiency in extraction and reaction in a system[37, 39–43].

”Ouzo effect” is when the ethanol and oil mixture is diluted with water and immediately becomes cloudy. This spontaneous emulsification in the ternary system is due to the oil solubility difference in the two solutions (water and alcohol). Oil is much more soluble in ethanol than in water, so small droplets form when more water is introduced into the system[44]. The solvent exchange method utilizes the Ouzo effect to produce high surface coverage of surface droplets with good reproducibility. According to Zhang et al.[29], there are three basic requirements for nanodroplets to form by solvent exchange. First, the two solvents in the ternary system must be

miscible with each other. Second, the liquid phase for the droplet must have a lower solubility in the second solvent than in the first solvent. Third, the substrate needs to have appropriate wettability for the droplet phase.

This section will cover the literature review on the topic of solvent exchange. First, the thesis will cover information on the liquid-liquid phase separation followed by a review of the parameters for controlling solvent exchange. Then, the theory and calculation behind the droplet growth and dissolution during the solvent exchange will be discussed. Next, the topic of the equipment that has been used in the literature for surface nanodroplet detection and measurement will be addressed.

### **2.1.2 Liquid-liquid phase separation (LLPS)**

Liquid-liquid phase separation (LLPS) is when a homogeneous solution demixes into two distinct liquid phases: a dense phase and a dilute phase[45]. Phase separation normally occurs when the Gibbs free energy of mixing is greater than zero or when Gibbs free energy is negative with respect to the unmixed components[14]. The phase separation can be achieved through changes in temperature, PH level, or composition. A phase diagram is often used to define the set of conditions that promotes the phase separation. For example, Figure 2.1 shows a typical phase diagram of macromolecules such as proteins or nucleic acids in water/organic solvent mixture. While in the two-phase regime, the two phases co-exist with the composition in the ends of a tie line[45]. The composition of the two phases does not change on the tie line, but the volume of the two phases may be calculated by using the reverse lever rule.

Within the phase diagram, there exist two curves known as binodal and spinodal curve as shown in Figure 2.1 (b). The binodal curve indicates the composition of two distinct phases at which they may co-exist. The spinodal curve indicates the region of instability where the spinodal decomposition, the phase separation without nucleation, occurs. The conditions between the binodal and spinodal curve is metastable, but phase separation may occur spontaneously, if the system can overcome an energy

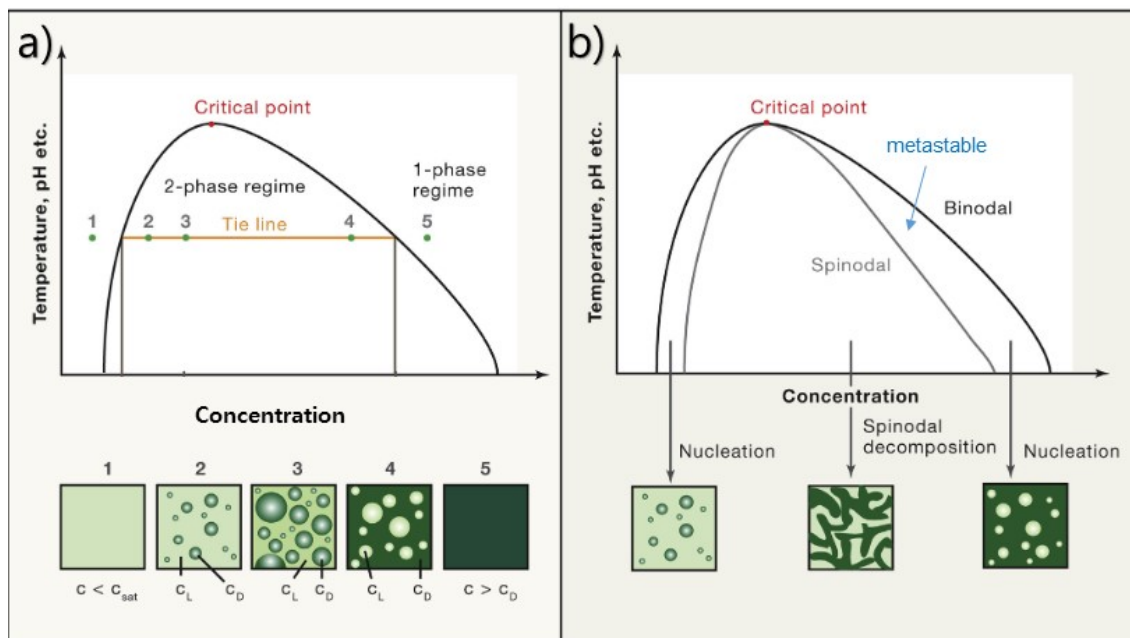


Figure 2.1: Typical phase diagram of macromolecules (i.e. proteins or nucleic acids) in water/organic solvent mixtures. a) The phase separation on the tie line. b) Binodal and spinodal curves with corresponding phase separation behaviour[45].  $C$  and  $C_{sat}$  are the concentration of the solution and the saturation concentration, respectively.  $D$  and  $L$  indicates the dense phase and the light phase within the two-phase regime

barrier[14]. Beyond the critical point, no phase separation can be observed[45].

### 2.1.3 Parameters for controlling the solvent exchange

For a solvent exchange process, various parameters can be adjusted for controlling the droplet formation. Main parameters include initial concentration, flow rate, channel height, and surface wettability[37]. These parameters are simple to change and allow droplet volume to be on a femtoliter or even attoliter scale[46]. As long as the three basic requirements for solvent exchange mentioned in the introduction are kept, various chemicals and materials can be used as the oil phase and the substrate.

#### Flow rate

The parameter that influences in mass transfer for solvent exchange is the flow rate. For the solvent exchange method, the flow rate controls the mixing between the two

solutions, which affects the overall droplet size. In the work of Zhang et al.[30], the final volume of surface nanodroplets increased with the flow rate. The theoretical model and experimental data showed a scaling law of the final volume of the droplets with the Peclet number  $Pe^{3/4}$ . The theoretical model for droplet growth will be discussed in detail in Section 2.1.4.

The droplet growth may be affected by the viscosity of the solution[33, 34]. For highly viscous solution, the final droplet size becomes less dependent to the external flow rate as droplet growth relies on the diffusion of oil and there is a critical value of flow rate at which the droplet size become independent of flow rate[34].

### **Initial solution composition**

Another important parameter for solvent exchange is the initial solution composition. For a given ternary system (i.e., ethanol, water, and cyclohexane ternary mixture), the solvent exchange would push the solution to go through a certain dilution path. This path is largely determined by the initial solution composition (solution A) and the bulk flow composition (solution B). This solution pair is typically chosen from the solution combination that has an Ouzo zone between the spinodal and binodal curves[44, 47]. During the solvent exchange, the concentration ratio between the droplet liquid and the good solvent is kept constant, and this is represented by the dilution curve. The area between the binodal curve and the dilution curve reflects the overall supersaturation generated by the solvent exchange process. The example of the droplet formation with varying initial solution composition is shown in Figure 2.2

### **Temperature**

The temperature has a significant effect on the solubility of the solute in the solution. For a certain initial concentration of a ternary solution, LLPS without mixing the antisolvent can be achieved through the manipulation of temperatures. In the work

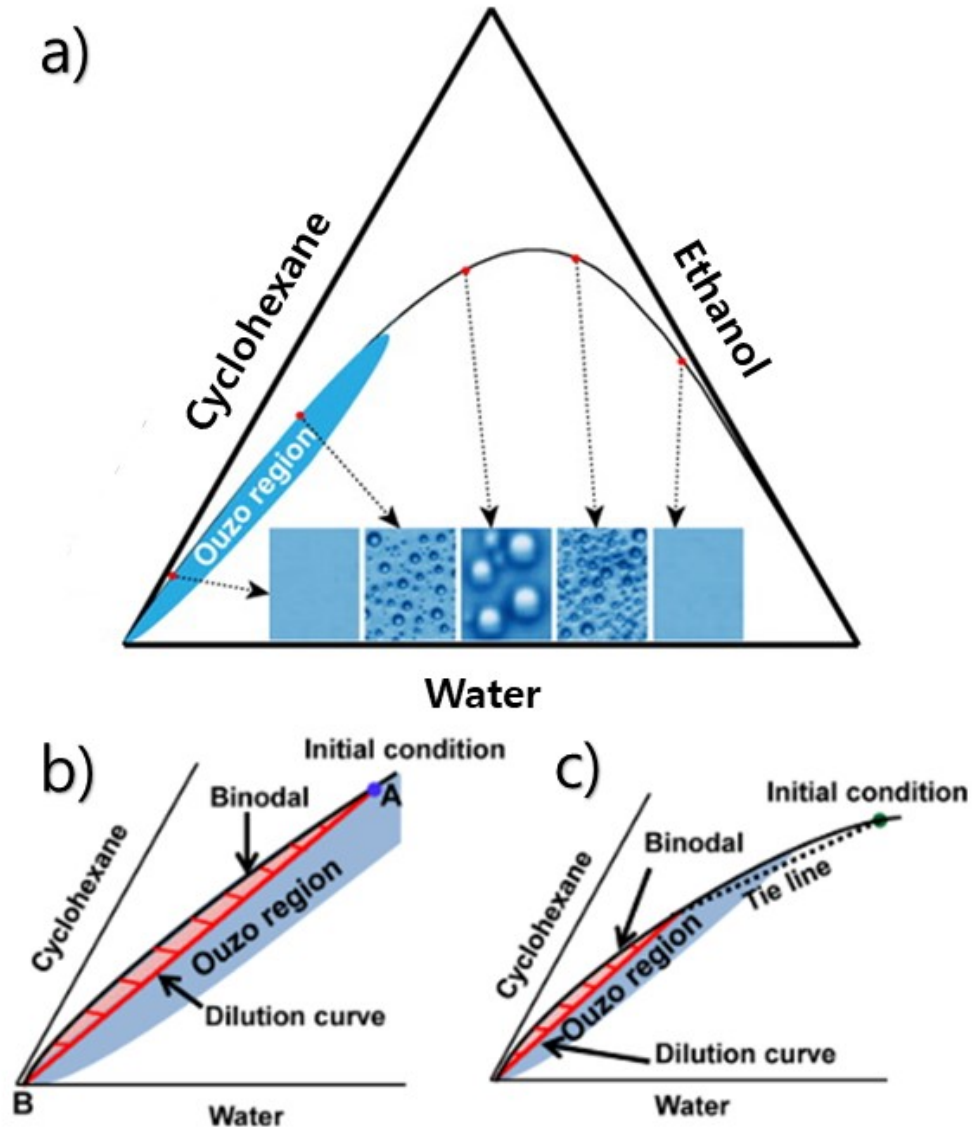


Figure 2.2: Three-phase diagram of cyclohexane, ethanol, and water. a) The ternary diagram with different droplet size depending on the initial solution composition. b), c) Sketch showing the composition during the solvent exchange on a dilution curve (red line). b) the initial solution start on the Ouzo region. c) the initial solution is out of the Ouzo region. the red shaded area indicates the supersaturation of the system[36].

of Guan et al.[48], the cold water was replaced by hot water through the solvent exchange method and created surface nanobubbles. The experiment indicated that the supersaturation is dependent on the different hot water temperatures as solution B. In theory, a combination of temperature differences of the solution A and B with

the addition of antisolvent can be used to optimize the droplet formation.

### **Channel height**

Channel height also affects the LLPS during the solvent exchange. For droplet formation by solvent exchange, the final volume of the droplet  $V_f$  increased with the channel height  $h$ , because the growth time of the droplets was longer in the higher channel height[30, 49]. At the same volumetric flow rate,  $V_f \sim h^3$  for the solvent exchange method.

As solution A (original solution) and solution B (incoming solution) have a difference in density, the gravity can cause the flow profile to shift[49]. This shift affects the concentration gradient that drives the droplet formation and leads to the difference in droplet formation on the top and bottom of the flow cell. For certain conditions, the convection roll would occur and enhance the mixing of the two solutions. Because the convection rolls are also driven by gravity, once the flow cell is set up horizontally, the difference between the channel height is no longer seen for solvent exchange[30].

In the cases of very small channel height, the droplet formation becomes diffusion-dominated as the Ouzo effect is confined to a quasi-2D channel[50]. In this situation, the droplets form a branching pattern as the new droplets only selectively nucleate behind the older ones[50]. The dendritic branching patterns of oil nanodroplets enhances the mobility of the colloidal particles and the effect was attributed to diffusiophoresis, a spontaneous motion induced by a concentration gradient[50].

Solvent exchange is not limited to rectangular cross-section channel. Other channels such as Hele-Shaw cell, cylindrical microtube cell, and a structured microchannel wall have been tested with solvent exchange[51–53]. In all cases, the final droplet size shows a universal 3/4 power law dependence on Peclet number  $Pe$  and the channel height  $h$ [51–53]. The droplet formation is strongly related to the local flow condition and is observed for controlled formation of surface nanodroplets on the microfiber where the local flow was disturbed by the curved surface[54].

## Surface wettability and micro-structures

The morphology of the surface droplet depends heavily on the wettability of the surface used in the solvent exchange[46]. A drop of liquid deposited on a substrate exhibits a contact angle depending on the surface properties according to Young’s law[55]. On a homogeneous surface, the solvent exchange method would obtain a large distribution in the droplet sizes with random positioning on the substrate[56].

The position and sizes of the droplet can be further controlled by the usage of micro-patterns of different surface wettability[46, 53]. More uniform droplet positioning has been achieved through selective nucleation, growth, and confinement of droplets with hydrophobic microdomains on the hydrophilic substrate[46, 53]. Through adjustment of the flow rate or oil concentration, the optimal droplet size can be achieved on the micro-patterned substrates[46, 53].

The micro-structures on the substrate affected the droplet morphology by providing a preferential nucleation site for droplet formation[53, 57–60]. With the cases for solvent exchange on micro-lens array on the substrate, the droplet nucleated on the rim of the micro-lens based on the interfacial energy minimization where the wettability of the micro-lenses and substrate material determined the droplet position and morphology[57–60]. The droplets on a micro-lens spontaneously form highly symmetrical arrangement as the diffusive interactions between the evolving droplets have preferential droplet number and the mean angle between the neighbouring droplets[57].

### 2.1.4 Growth and dissolution dynamics of droplets

#### The morphology of surface droplets

The morphology of the surface droplets is based on Young’s equation[30]. The Young’s equation is defined as:

$$\cos(\theta) = \frac{\sigma_{SL_1} - \sigma_{SL_2}}{\sigma_{L_1L_2}} \quad (2.1)$$

where  $\theta$  is the contact angle of the surface droplet in Solution B and  $\sigma$  is the surface tensions for the solid-liquid (surrounding solution), solid-liquid (droplet), and liquid-liquid interfaces.  $L_1$  is the liquid phase of the droplets,  $L_2$  is the liquid phase of the surrounding, and  $S$  is the solid surface where the surface droplet grows or dissolves. The morphology of the surface droplet is shown in Figure 2.3.

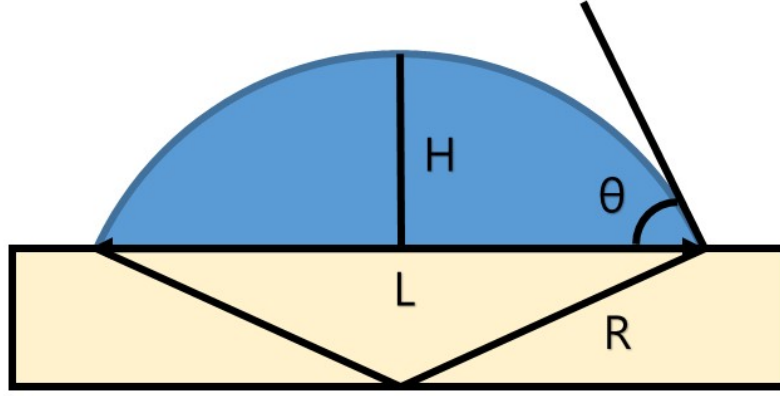


Figure 2.3: The morphology of the surface droplet.

This contact angle is used to also define the volume and surface area of the droplets. By assuming that the droplets are in the shape of the spherical-cap, the height of the droplet  $H$ , can be defined by using the footprint diameter  $L$ .

$$H = \frac{1 - \cos(\theta)}{2\sin(\theta)}L \quad (2.2)$$

The volume  $V$  and the surface area  $A$  of the droplet are defined as:

$$V = \frac{\pi}{24}H(3L^2 + 4H^2) \quad (2.3)$$

$$A = \frac{\pi}{4}(L^2 + 4H^2) \quad (2.4)$$

And the radius of curvature is defined as:

$$R = \frac{L}{2\sin(\theta)} \quad (2.5)$$

### **The mass transfer during the growth or dissolution of a surface droplet**

The transportation of the oil phase for a droplet can be defined as a function of time. For the equation, we assume that the diffusion of the solute in or out of the droplet is the rate-determining mechanism. By using Fick's law,  $J = -D\Delta c$  where  $\Delta c = (c_\infty - c_s)$ , we can come to equation 2.6.

$$\frac{dM}{dt} = \frac{\pi}{2}LD \cdot (c_\infty - c_s) \cdot f(\theta) \quad (2.6)$$

The mass of the solute is defined as  $M$ , and  $c_\infty$  and  $c_s$  are the concentration of solute in the surrounding liquid and the concentration at the interface.  $f(\theta)$  is a geometric function and is defined as:

$$f(\theta) = \frac{\sin(\theta)}{1 + \cos(\theta)} + 4 \int_0^\infty \frac{1 + \cosh(2\theta\zeta)}{\sinh(2\pi\zeta)} \tanh[(\pi - \theta)\zeta] d\zeta \quad (2.7)$$

During the solvent exchange, the droplet may grow or dissolve in three possible manners: Constant contact angle mode (CA mode), constant radius mode (CR mode), and any combination of these two modes (mixed mode)[56]. The schemes of different surface droplet dissolution are shown in Figure 2.4.

### **Different modes of droplet growth or dissolution: Constant Radius (CR) mode**

For CR mode, the droplet contact line is pinned to the surface so the contact angle is changing with time. Equation 2.6 is reduced to

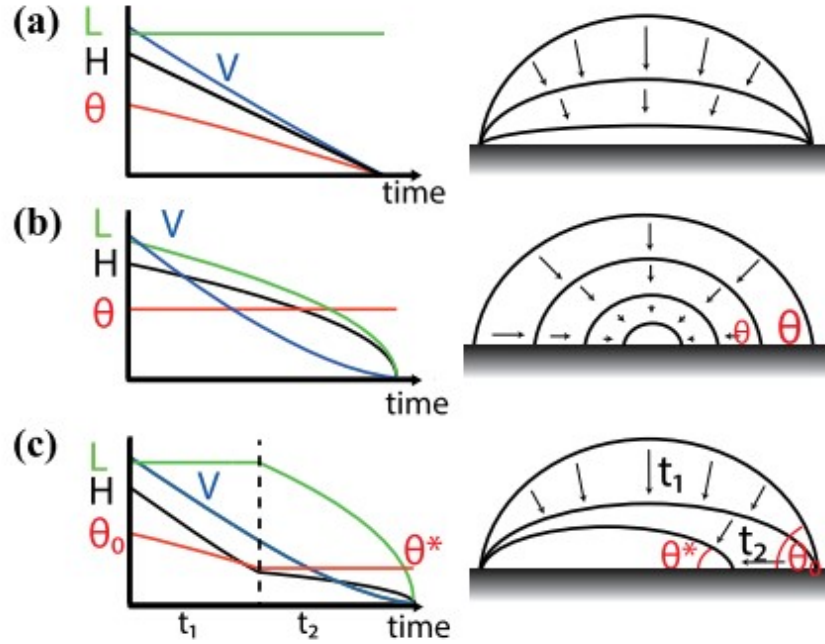


Figure 2.4: Schemes of surface droplet dissolution modes. a) CR mode, b) CA mode, c) Stick-slide mode, i.e., the droplet dissolves in an iteration of CR and CA modes.[56]

$$\frac{d\theta}{dt} = \frac{4D(c_s - c_\infty)}{\rho L^2} (1 + \cos(\theta))^2 f(\theta) \quad (2.8)$$

The CR mode droplet growth/dissolution is often observed for pinned contact line where the droplet radius has to be constant. Therefore this mode is used to study the behaviour on patterned or micro-structured surfaces during the solvent exchange process.

### Different modes of droplet growth or dissolution: Constant angle (CA) mode

For CA mode, the contact angle is constant so the equation can be reduced to

$$L \frac{dL}{dt} = \frac{4D(c_s - c_\infty)}{\rho} \frac{f(\theta)}{3g(\theta)} \quad (2.9)$$

where  $g(\theta)$  is a geometrical function. Equation 2.9 can be further integrated to obtain the lateral diameter of the surface droplet as a function of time.

$$L(t) = (L_0^2 - \frac{8D(c_s - c_\infty)}{\rho} \frac{f(\theta)}{3g(\theta)} t)^{1/2} \quad (2.10)$$

$L_0$  is the initial lateral diameter of the droplet.

### Growth of droplets solvent exchange method

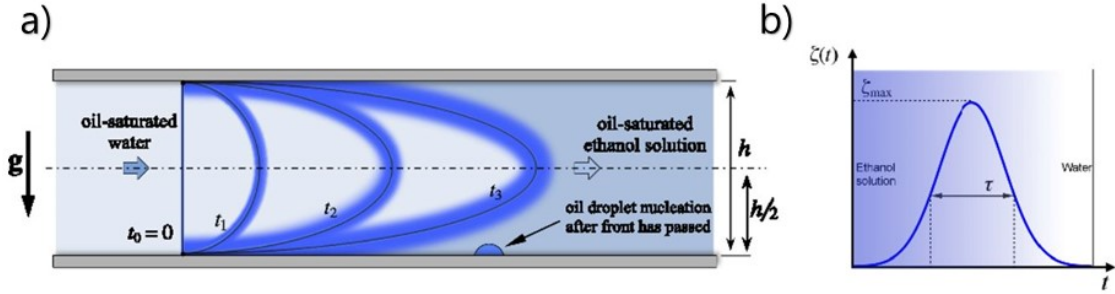


Figure 2.5: a) Parabolic flow profiles for various times. no-slip boundary condition for the flow is applied. b) Approximate evolution of the oversaturation  $\zeta(t)$  at fixed position.  $\tau$  is the width of the oversaturation pulse[30].

Solvent exchange does not use mixing through an agitator but through a pulse of solute oversaturation created by the mixing front[30, 32] (Figure 2.5). The oversaturation  $\zeta(t)$  at fixed position have  $\zeta_{max}$  as the highest oversaturation point.  $\tau$  is the width of the oversaturation pulse defined by  $\int_0^\infty \zeta(t) dt = \zeta_{max}\tau$ . Using the assumption  $\tau \sim h^2/D$ , the final droplet size has shown to have a scaling law with the dimensionless number called Peclet number ( $Pe$ ).

$$V \sim h^3 \left( \frac{c_{sat,poor}}{\rho} \right)^{3/2} \left( \frac{c_{sat,good}}{c_{sat,poor}} - 1 \right) Pe^{3/4} \quad (2.11)$$

Where  $V$ ,  $h$ , and  $\rho$  are the droplet volume, channel height, and the density of the fluid.  $c_{sat,poor}$  and  $c_{sat,good}$  are the saturation concentration of solute in the poor solvent

and the good solvent. Peclet number is a dimensionless number that represents the ratio of mass transfer by the motion of the fluid to mass transfer by diffusion. The dimensionless number Peclet number is defined as:

$$Pe = \frac{\bar{U}h}{D} = \frac{Q}{wD} \quad (2.12)$$

where  $Q$  is the volumeric flow rate,  $w$  is the channel width, and  $D$  the diffusion coefficient.

### **Effects of gravity on the solvent exchange process**

The effects of gravity may have a significant effect on the droplet formation during solvent exchange[30, 49]. The gravity shifted the parabolic profile of the moving front due to the density difference between the two solutions (Figure 2.6)[49]. Archimedes number  $Ar$  is a crucial control parameter in controlling the gravity effect and is affected by channel height as

$$Ar = \frac{g(h)^3 \Delta\rho}{\nu^2 \rho} \quad (2.13)$$

where  $\Delta \rho$  is the density difference between the two solutions, the gravitational acceleration  $g$  is  $9.8 \text{ m/s}^2$ , and  $\nu$  is kinematic viscosity of the incoming solution. For  $Ar \gg 1$ , the gravity plays a prominent role but for  $Ar \ll 1$ , the gravity effect can be neglected.

Depending on the channel height the enhanced mixing from convection may occur[30, 49]. The density difference between solution A and solution B is the key to the onset of convection rolls. To estimate when the convection rolls set in due to the density difference, we calculate Rayleigh number  $Ra$ .

$$Ra = \frac{\Delta\rho g(h/2)^3}{\mu D} \quad (2.14)$$

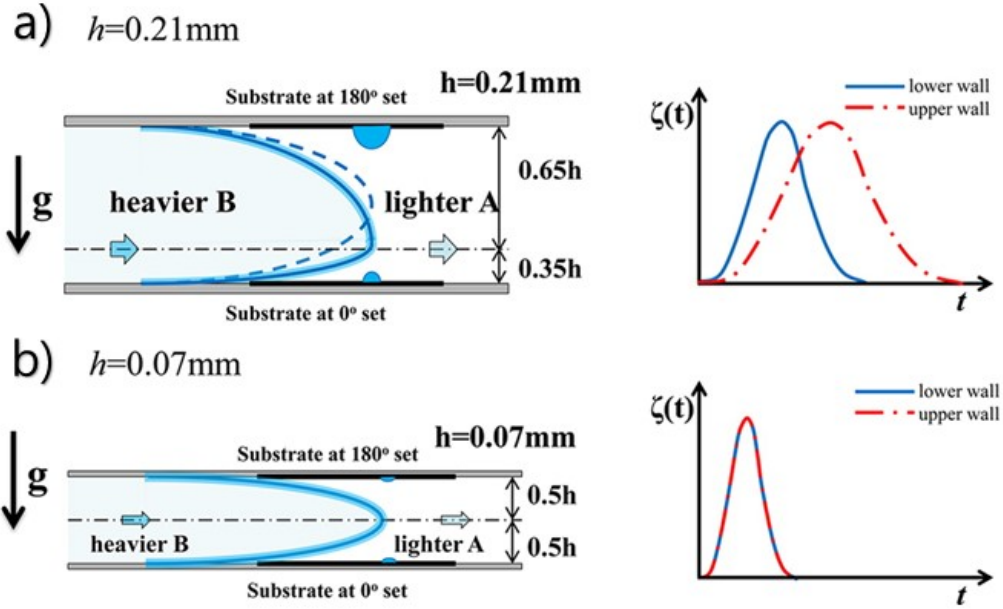


Figure 2.6: Flow profile shift due to gravity during solvent exchange. a) flow profile and oversaturation pulse for  $Ar \gg 1$  b) flow profile and oversaturation pulse for  $Ar \ll 1$ [49].

Here  $\mu$  is the dynamic viscosity of solution A and  $D$  is the mass diffusion coefficient. The convection roll may occur when the Rayleigh number is larger than the critical Rayleigh number 1,708[61].

## 2.2 Techniques used in the literature for surface droplet measurement

There are many techniques available for detecting and measuring the surface nanodroplets. Certain techniques such as atomic force microscopy (AFM) would have a high spatial resolution but takes a long time. Other techniques such as Fourier transform infrared (FTIR) spectroscopy are sensitive to the chemical properties. Optical microscopy and other techniques are fast and non-intrusive. To acquire better characterization of the droplet and the process of droplet formation, combinations of complementary techniques are used. However, the difficult task of acquiring high spatial resolution along with good temporal resolution and chemical identification at

Type	Advantages	Disadvantages
Atomic force microscopy (AFM) [29–31, 35, 37, 46, 47, 50, 53, 59]	3D resolution and measurement can be acquired	Intrusive, slow and chemically blind
Optical microscopy [28, 30, 36, 46, 47, 50, 56, 62, 63]	Non-intrusive and fast	Limited to microscale observation
Attenuated total internal reflection (ATR) [28, 35, 38, 64]	Non-intrusive and highly sensitive to the sample. ATR can be applied in combination with fluorescence spectroscopy (TIRF), and Fourier transform infrared (FTIR)	Limited to specific experiment set up and conditions
Raman spectroscopy [37, 62]	Sensitive to chemicals and applicable to aqueous environment	Need nanostructures to enhance the signal
Surface plasmon resonance spectroscopy [65, 66]	Less intrusive than AFM and have high sensitivity	Low spatial resolution
Quartz crystal microbalance [67, 68]	Highly sensitive to the sample with fast time scale	Low spatial resolution

Table 2.1: List of techniques to observe surface droplets[28]

the same time still exists[28]. Table 2.1 lists the wide range of techniques for surface droplet observation with the advantages and disadvantages for each technique.

## 2.3 Crystallization of classical nucleation and oiling-out phenomenon

### 2.3.1 Introduction

Crystallization is one of the oldest unit operations and is involved in several industries as one of the most important processes. The reason why crystallization is widely used for various materials is that the product from this technique has high purification

potential and the crystalline material can be easy to separate through filtration[69]. There are many techniques to achieve crystallization and certain combinations of different techniques allow more intricate control over the process. Crystallization is used in various industries traditionally from foods, metallurgy, geology, physiology, pharmaceutical industries, and even new applications in electronics and surface treatments.[69–71]

Crystallization occurs in three major steps: supersaturation event, nucleation event, and crystal growth[69]. The supersaturation event occurs when the solution has increased in solute concentration or decrease in solute solubility through reaction, evaporation, mixing, or cooling[69]. The nucleation event occurs once the supersaturated solution has random assembling of molecules and forms stable solid interfaces. During this event, the material has to reach a critical crystal size to be in the stable crystalline form[69]. The crystal growth occurs as these nucleated seeds start to grow in size and mature to attain reduce the solution back to the saturated state[69].

This subsection will cover the basics of crystallization mostly based on a textbook[69]. First, the literature review will cover the different types of common crystallization. This section will then review the crystalline structure and the equipment used for studying crystallization. The classical theory on crystallization (non-oiling-out) will be covered before discussing further into oiling-out crystallization.

### **2.3.2 Common types of crystallization**

Crystallization can be applied to many different fields and applications. Along with the many different uses comes different ways to utilize the crystallization. Common crystallization techniques that can be seen in many industries are solution, precipitation, and melt crystallization[69]. There are other more advanced techniques such as salting in/out, co-crystallization, racemic crystallization, and others[72].

## **Solution Crystallization**

Solution crystallization is a technique that involves achieving supersaturation through concentration and solubility changes from a single-phase solution[69]. Within the solution crystallization, we can even further divide into evaporating, cooling, and vacuum crystallizing.

## **Precipitation**

Precipitation involves the addition of another chemical to achieve the necessary supersaturation for nucleation. This addition of different chemicals would result in fast nucleation and the formation of small crystals[69, 73]. Precipitation may be formed through reaction or addition of antisolvent. Crystallization through the solvent exchange method would fall into the non-reactive precipitation category.

## **Melt Crystallization**

The term "melt" is generally used for referring to a liquid close to the freezing point. The main advantage of melt crystallization is the low energy demand as the latent heat of vaporization requires more energy than the latent heat of fusion[69].

### **2.3.3 Crystalline structure and equipment for crystal studies**

When a material crystallizes, the crystals have few organized rigid structures with specific symmetry in axis, plane, and centre[69]. The three-dimensional arrangement of the crystal structures is called elementary cells[70]. Often, the shapes of the crystals in macroscopic scale match the atomic crystalline structures so the crystal structures can often be determined by visual or microscopic observation. For more precise measurement, X-ray crystallography is often used for measuring and classifying the crystals[73].

Certain materials have the ability to exist in different crystal structures and are known as polymorphs. Different crystal structures of polymorphs can have differences

in density, solubility, melting points, and reactivity even though the crystals are chemically identical[8, 69]. Each polymorph is considered to be a different phase and a polymorph may transition into different polymorphs depending on the temperature and pressure[69]. As many drugs in the pharmaceutical industry have substances with more than one crystalline form, the research continues to find, identify, and characterize the polymorphic substances.[74, 75]

Techniques	Principles	Application
Focused beam reflectance measurement (FBRM)	Measures the chord length by calculating the light speed and the time of the reflected laser.	Particle size distribution
Particle video microscope (PVM)	Takes high resolution video and measures the scattering effect of multiple laser lights from the probe.	In-situ image of crystals
ATR - fourier transformed infrared (FTIR)	Enhances the absorption of infrared spectrum by using a thin crystal medium.	Concentration and polymorphs
ATR - ultraviolet and visible spectrophotometer (UV/Vis)	Enhances the absorption of UV-Vis spectrum by using a thin crystal medium.	Nucleation event and polymorphic transition
Raman spectra	Uses Raman spectra based on Raman scattering to detect molecular vibration and rotation.	Crystal structure and polymorphism
X-ray powder diffraction (XRD)	Measures the intensity of the X-ray diffraction while the sample and the detector are being rotated.	Crystal structure and purity of the sample.
Differential scanning calorimetry (DSC)	Measures the heat required to increase the temperature of the sample.	Phase transition and changes in heat capacity.

Table 2.2: List of techniques for observing crystallization and crystal products[76]

There are many techniques for the characterization of the crystals and the crystallization process[76]. Table 2.2 shows techniques for observing the crystallization

processes and the crystal products. For gathering information about the crystallization process, focused beam reflectance measurement (FBRM) and particle video microscope (PVM) are used in conjunction as a part of process analytical technologies (PAT). The details on the crystal growth rate and crystal shape can be acquired in real-time. Various electromagnetic spectrum (infrared, visible, ultraviolet, and Raman) can be used to identify the sample but often the signal can be too weak[77]. The signal can be enhanced by using a thin layer of attenuated total reflection (ATR) crystals and allow the crystallization process to be measured in real-time. X-ray powder diffraction (XRD) and differential scanning calorimetry (DSC) both provide valuable information about the crystal structure and the crystal properties but they do not provide information about the process of the crystallization. Many studies use multiple techniques to gather more precise information about the crystallization process and the crystal product.

### **2.3.4 Classical nucleation theory (CNT)**

When a solution reaches supersaturation, crystallization can be induced. The nucleation, the formation of stable nuclei, is the rate-determining step for crystallization as the solution may remain as a metastable phase for long periods of time depending on the supersaturation level[69]. To induce crystallization, an artificial method such as agitation, friction, mechanical shock, cavitation, and high pressure can be used[69].

The spontaneous nucleation can be modeled using classical nucleation theory (CNT). The Gibbs free energy of the crystallization system has two competing terms: the interfacial energy and bulk energy[69, 70]. The interfacial energy is associated with the creation of the new interface and is thermodynamically unfavorable. The bulk energy is associated with the creation of volume of the nucleus and is thermodynamically favorable. As the surface tension of a sphere has the lowest interfacial energy demand, the nuclei is assumed to be in a spherical shape[78]. The relation of the free energy curves in CNT model is shown in Figure 2.7

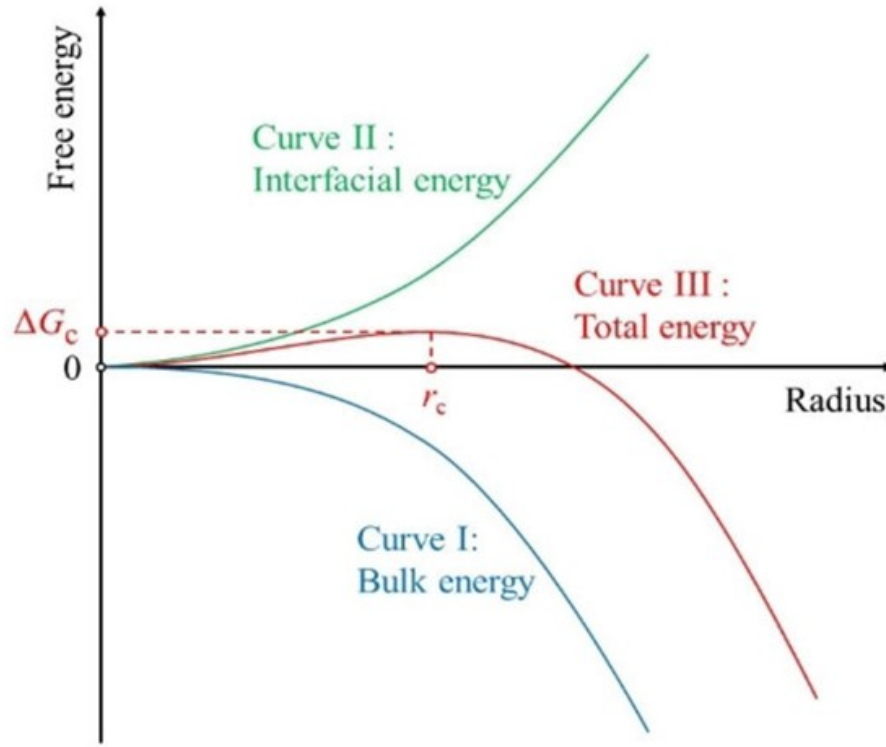


Figure 2.7: The relation of interfacial energy, bulk energy, and the total free energy in classical nucleation theory (CNT)[76, 79].  $\Delta G_c$  indicates the energy barrier for spontaneous crystallization at critical radius  $r_c$ . The nucleus smaller than the critical radius is unstable therefore will dissolve spontaneously[69].

### 2.3.5 Heterogenous nucleation on solid surface

The presence of a foreign surface can induce nucleation at a lower supersaturation condition than those required for spontaneous nucleation[69, 78]. This is because the Gibbs free energy for the formation of critical nucleus under heterogeneous conditions  $\Delta G'_c$  is lower than condition under homogeneous nucleation. A numerical factor  $\phi$  can be used to define the Gibbs free energy of two conditions as Equation 2.15.

$$\Delta G'_c = \phi \Delta G_c \quad (2.15)$$

Depending on the affinity between the crystalline solid and the foreign solid surface, the crystal nucleation can be induced and this affinity is represented by the contact

angle  $\theta$  in the Young's law [69, 78]. For complete non-wetting ( $\theta = 180^\circ$ ), the overall free energy of nucleation is the same as that required for homogeneous nucleation. For complete wetting ( $\theta = 0$ ), the case corresponds to seeded supersaturated solution where no nuclei have to be formed for crystal growth [69]. Figure 2.8 indicates the relationship between  $\phi$  and  $\theta$ .

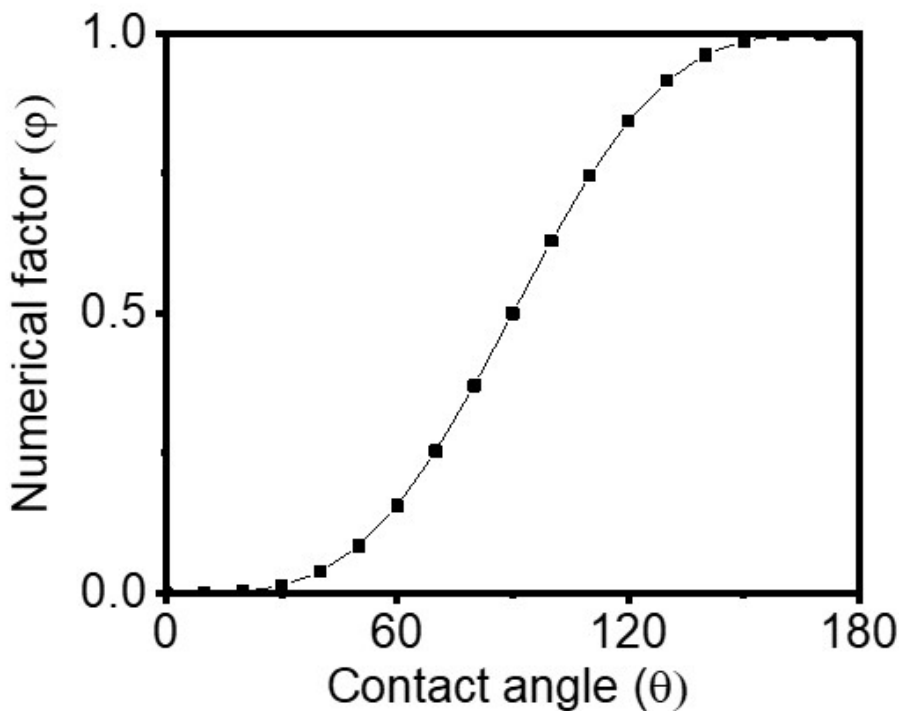


Figure 2.8: Heterogeneous nucleation and the relation to surface contact angle [69, 78]

### 2.3.6 Oiling-out crystallization

Within the process of crystallization, some chemicals may encounter a phenomenon known as oiling-out. The list of substances with oiling-out phenomenon in the literature is shown in Table 2.3. The oiling-out phenomenon would cause a secondary liquid phase to form and would in turn hinder the crystal nucleation and its growth [3, 8]. Not only that, the oil phase created by this phenomenon usually has higher solubility

to the impurities which may create poor quality crystal products. This undermines purification, which is the most important aspect of crystallization, and causes significant problems when the process is scaled up to industrial production[3].

There is no generally accepted conclusion about the causes of oiling-out crystallization as there is still a large dispute about the physical mechanism behind the oiling-out[76]. However, there are experimental investigations of the influence factors of oiling-out crystallization. These factors include molecular properties of solutes[1, 3], solvents[2, 12, 87], supersaturation[7, 11, 25, 85], the concentration of solutes[8, 21, 80], temperature[21, 23], and foreign substances[27].

As mentioned, there are adverse effects of oiling-out so there are many ways developed by the researchers to avoid the oiling-out phenomenon[3]. Optimizing the initial conditions of the crystallization system such as choosing appropriate initial concentrations, solvents, and improving the purity of the raw material can improve the crystallization for an oiling-out system[8, 12, 88]. Seeding can induce the crystallization and inhibit droplet nucleation[11, 25]. Another way is to use ultrasound to create cavitation, thermal, and mechanical effects to induce crystallization and inhibit oiling-out[89, 90]. For cooling crystallization, the cooling rate can be slowed to avoid the oiling-out phenomenon[91].

### **2.3.7 Two-step nucleation theory**

The oiling-out crystallization behaviour significantly deviates from the classical nucleation theory. Therefore, Vekilov suggested an alternative nucleation mechanism for oiling-out crystallization and named it “two-step nucleation mechanism”[92]. The two-step nucleation has the dense liquid droplet nucleate first and then the crystal nucleus forms inside the droplet. According to Vekilov, all nucleation process includes at least two steps as shown in Figure 2.9 (b). The oiling-out phenomenon results from the difference of the free energy minimum between the initial phase (initial solution) and the intermediate phase (dense secondary liquid). The formation free energy of

Substance	Solvents/mixtures	Reference
Beta-alanine	Water-ethanol	(Sun et al., 2018)[21, 23]
Butyl paraben	Water-ethanol	(Yang et al., 2016)[80]
Vanillin	Water-1-propanol Water	(Du et al., 2016)[12] (Albuquerque and Mazzotti, 2014)[71]
Idebenone	Hexane-methylene chlorine	(Lu et al., 2012)[8]
Lauric acid	Water-ethanol	(Maeda et al., 2001)[81]
Polyethylenglycoldimethyl - ether (PEGDME)	2-Propanol, diethylke- tone, ethyl acetate	(Kiesow et al., 2016)[1]
Pyraclostrobin	Isopropanol - cyclohex- ane	(Li et al., 2016)[82]
$C_{35}H_{41}Cl_2N_3O_2$	Water-ethanol	(Lafferrer et al., 2004)[2]
Erythromycin ethylsuccinate	Tetrahydrofuran (THF)-water	(Li et al., 2016)[82]
API	Water-ethanol	(Veesler et al., 2006)[83]
API-T	Acetone-water	(Takasuga and Ooshima, 2015)[5]
Antiandrogen	n-heptane	(Daver et al., 2016)[84]
Methyl(E) - 2 - [2 - (6 - trifluoromethylpyridine - 2 - yloxymethyl) - phenyl] - 3 - methoxyacrylate	Water-methanol	(Bonnett et al., 2003)[85]
Bristol-Myers Squibb drug	Ethyl acetate - cyclo- hexane, water-ethanol	(kim et al., 2003)[86]
4,4' dihydroxydiphenylsul- fone (DHDPS)	Water-acetone, water- isopropanol	(Kiesow et al., 2018)[87]

Table 2.3: Example substances with oiling-out crystallization behaviour from the literature

the dense metastable liquid phase  $\Delta G_{L-L}$  is negative for oiling-out crystallization.

The classical nucleation would have a positive value of  $\Delta G_{L-L}$ .

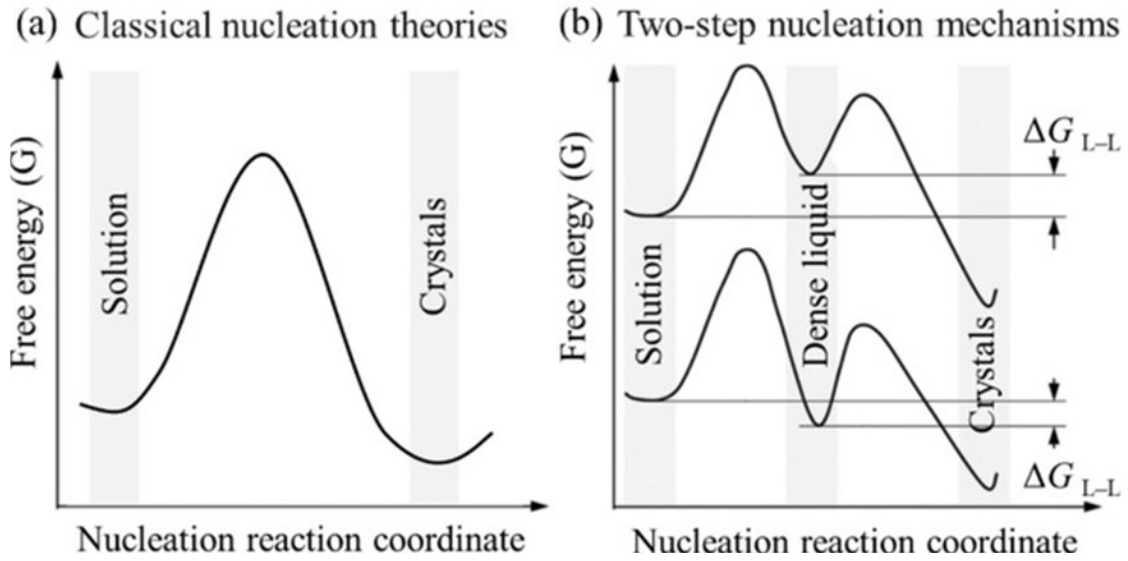


Figure 2.9: Schematic diagrams of the free energy of a) CNT and b) the two-step nucleation theory.[76, 92]

The two-step nucleation theory interprets the molecular behaviour during the nucleation as density fluctuation and structural transformation[92]. In Figure 2.10, the molecules of the solute form dense and disordered clusters. As the process is reversible, the density of the clusters fluctuates as a critical size of the liquid nucleus is achieved. The second step of structural transformation organizes the disordered clusters into an organized crystalline nucleus. For one-step nucleation (CNT), the molecules would experience both of the steps simultaneously and proceed as calculations of CNT predicts.

The two-step nucleation theory can explain the behaviour for system with the formation of disordered clusters. However, there has been oiling-out system where the crystallization occurs in the continuous phase rather than in the oil droplets[76]. Davey et al. reported that crystal nucleation in theory should be able to occur in either liquid phases[93]. This is inconsistent with the two-step nucleation theory as what Vekilov states is the nucleation of liquid cluster becomes the nucleus of the crystal. Also, there has been reports of LLPS in inorganic system which is different from either CNT and two-step nucleation[76, 94]. So further researches are needed

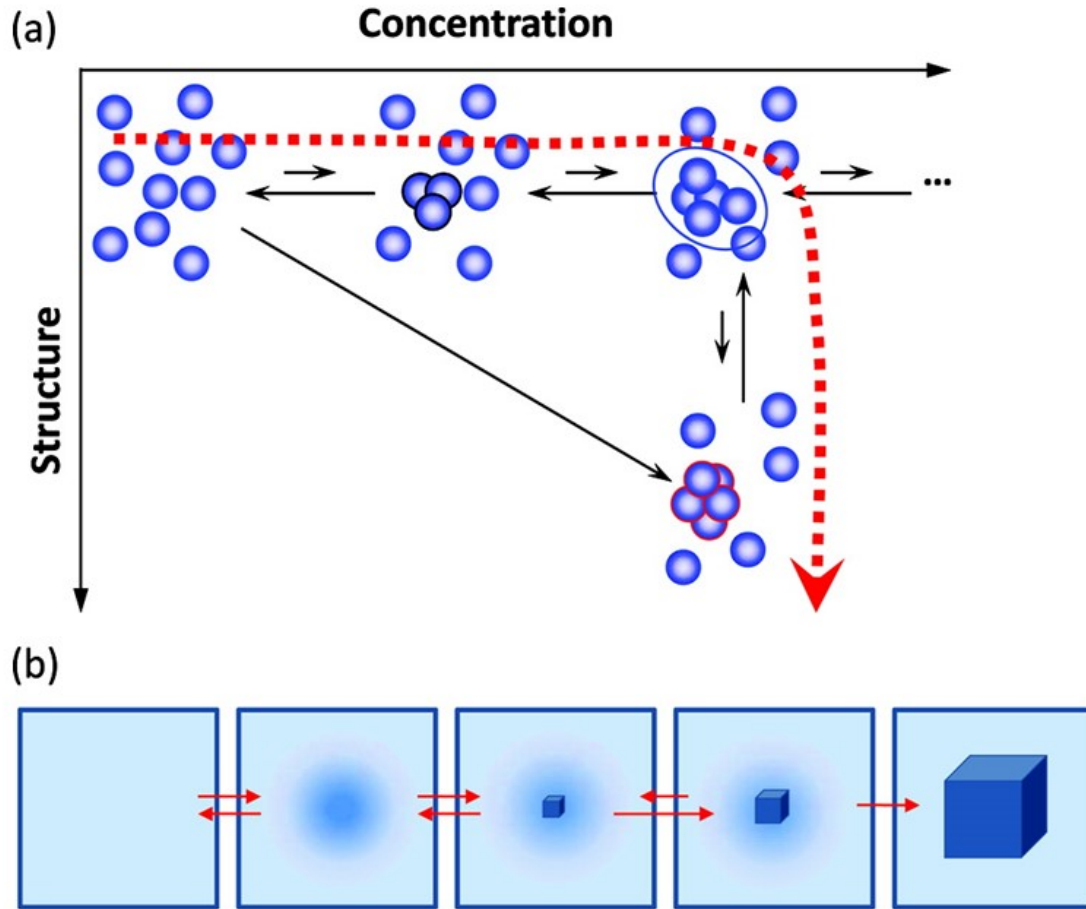


Figure 2.10: Schematic diagrams of the two-step nucleation theory. a) Microscopic view point in the (concentration, structure) plane and b) macroscopic view point of the events along the dashed arrow curve. the the solid arrow line indicates the one-step nucleation and the dashed arrow curve indicates the two-step nucleation.[79, 92]

regarding to the oiling-out crystallization and the universal theory on the mechanism.

### 2.3.8 Counter diffusion of oiling-out droplet crystallization

Counter diffusion occurs when two chemicals diffuse in opposite directions to achieve the equilibrium. This is often observed in the quasi-emulsion solvent diffusion (QESD). QESD is one of the ways to form spherical agglomerates of crystals by utilizing the oiling-out phenomenon[95, 96]. In the process, the solvent phase (solute dissolved in a solvent) is added to the antisolvent solution under agitation (Figure

2.11). The solvent is dispersed in the antisolvent and creates quasi-emulsion, the formation of unstable emulsion[96]. As soon as the emulsion is formed, counter diffusion occurs where the solvent and antisolvent diffuse in opposite directions. The solubility of the solute is reduced as the antisolvent diffuses into the droplets and induces crystallization inside the droplets[21].

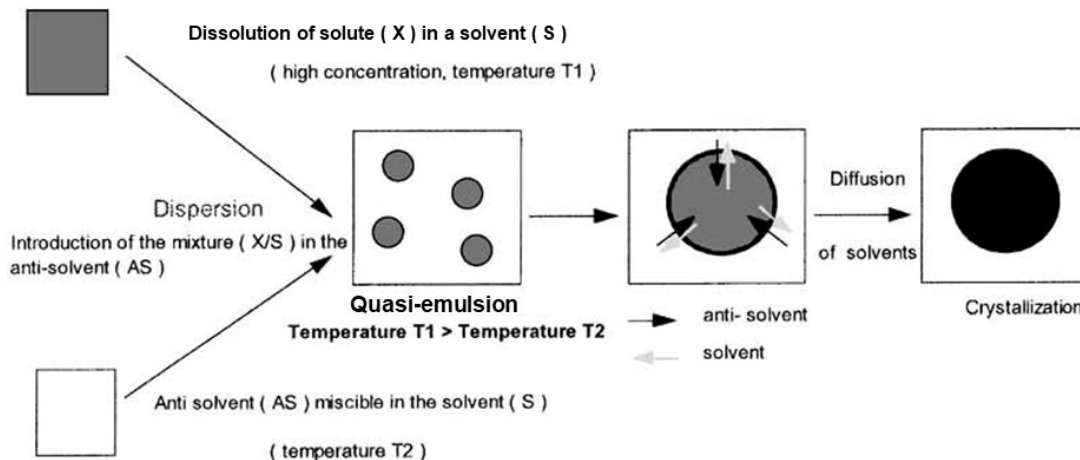


Figure 2.11: Diagrams of spherical crystallization process by quasi-emulsion solvent diffusion (QESD) method[96]

## 2.4 Conclusions

In conclusion, the solvent exchange method has been shown to have reproducible results with simple parameters to control the size, quantity, and morphology of the droplets. If the correct conditions for LLPS can be met, the solvent exchange has shown various advantages in controlling surface droplet formation. Current literature provided the mechanism and theory behind the solvent exchange method and the equipment that could support the findings. By utilizing the information in the literature, various applications for surface droplets had been tested and proven to be effective. Therefore, the solvent exchange method was used for studying the behaviour of oiling-out crystallization in our works. As the understandings of solvent

exchange mechanism develop better optimization, new and exciting applications of surface nanodroplets are surely to come in the future.

Crystallization has been a valuable method for purification and separation for centuries. Along with the centuries of practices came a greater understanding of the crystalline systems and their crystallization processes. With new techniques that can capture the process in real-time, more difficult phenomena have been tackled by the researchers. One of the difficult phenomena currently standing in the field of crystallization is the oiling-out phenomenon. The formation of a new liquid phase delays the crystal nucleation process and causes the previous theory on crystallization (CNT) to be impractical. Therefore, a more recent theory of two-step nucleation has been developed. However, there are a few oiling-out crystallization systems where two-step nucleation is not congruent with the phenomenon. Therefore, further research of the oiling-out crystallization phenomenon with the solvent exchange method would provide new insight into the disputed mechanisms.

## **2.5 Knowledge gaps in research on oiling-out crystallization**

As mentioned, the mechanism for oiling-out crystallization is still in discussion among the researchers. Therefore, utilizing effective ways to control and study the oiling-out crystallization is necessary. Both crystallization and solvent exchange methods have been extensively studied by many researchers in the literature. However, using the solvent exchange method to study the crystallization has not been researched yet. Connecting the two fields of researches would be beneficial for understanding the mechanisms and processes of oiling-out crystallization. With more experimentation, new substances that exhibit the oiling-out phenomenon can be found and studied to close many gaps in the research. On the other hand, the solvent exchange method and the theory behind the dynamics of nucleation may benefit in more diverse applications which may bring more collaboration with other subfields of science.

# Chapter 3

## Methods and procedure

### 3.1 Substrate preparation

The bare silicon substrates and silicon dioxide substrates were purchased from University Wafer (South Boston, MA, US). To prepare the experiment, 300 nm wet thermal oxide  $SiO_2$  wafer was cleansed by sonication in deionized water (from Milli-Q Direct) and then in ethanol for 10-20 minutes each before use. The bare silicon substrate was cleansed by piranha solution for 10-20 minutes at 75 °C by a hot plate then sonicated by deionized water for 10-20 minutes. The substrates were cut manually by a hand scribe then cleaned by sonication in deionized water (from Milli-Q Direct) and ethanol for 10-20 minutes each before use. The substrate were dried by compressed air before being placed in the flow cell with a double sided tape.

For hydrophobized substrates, octadecyl trichlorosilane (OTS) coatings were used on bare silicon substrate[97]. After the bare silicon substrate was cleansed by piranha solution and sonication in water, the substrate was put into an oven for an hour at 120 °C to remove the moisture. If some residues from the impurity were observed, sonication under deionized water was repeated and dried in oven until the substrate was visibly clean. Once the substrate was dried and cooled, the clean wafer was submerged in 0.5 vol% of OTS (Alfa Aesar, 99.9%) in hexane (Fisher Scientific, 99.9%) at room temperature for 12 hours in a sealed container to avoid the moisture. Once the coating was complete, the substrate was sonicated by hexane, acetone, and ethanol, each

by 10 minutes. The substrate was cut manually by a hand scribe and were washed and sonicated in deionized water for 10 min before use. 3-aminopropyltriethoxysilane (APTES) coated substrates were prepared in a similar manner as the OTS coated substrates. After the wafer was completely dry from cleaning, the substrate was submerged in 1.5 vol% of APTES (Alfa Aesar, 99.9%) in toluene (Fisher Scientific, 99.9%) for 1.5 hours in a sealed container. Once the coating was completed, the substrate was sonicated by ethanol and water.

The OTS coated wafer was used as the bases for fabricating the patterned substrate via standard photolithography followed by plasma etching[46, 64]. On the OTS-treated wafer, a layer of positive photoresist (AZ1529, EMD Performance Materials, Germany) was spin-coated at a thickness of 4  $\mu\text{m}$  and baked at 100 °C for 1 min. Subsequently, the photoresist-coated wafer was exposed under UV light using a mask aligner (ABM, USA) through a photomask containing the pattern. After exposure, the pattern was developed in AZ400K developer (AZ Electronic Materials, USA) diluted with de-ionized water at a ratio of developer : water = 1 : 4. Following the photoresist development, the exposed surface was turned hydrophilic by an  $O_2$  descum process using a reactive ion etching (RIE) system (Trion technology, USA). Finally, the unexposed photoresist was removed in acetone to reveal the un-etched hydrophobic patterns and then they were sonicated in water and ethanol before use. These patterned substrates also became bases for 1, 6-hexanediol diacrylate (HDODA) lens array which was polymerized after solvent exchange as mentioned in the works of Bao et al.[46] While the lens were largely confined to the pattern with uniform sizes and positions, some irregularities did exist. The patterned substrates and polymer lens arrays were used in the experiments for Chapter 5.

The contact angle of the water droplet in air was measured for APTES and the contact angle was approximately 50-60 degrees. The contact angle from hydrophilic and hydrophobic components of the patterned substrate was approximately 20-30 and 100-110 degrees, respectively.

## 3.2 Solution preparation

Beta-alanine (ACROS organics, 99 %), ethanol (Fisher Scientific, HPLC Grade, including 90 % ethanol, 5 % methanol, 5 % isopropanol), isopropanol (IPA, Fisher Scientific, 99.9 %) were mainly used for solution preparation. The solution was stored in a sealed container for overnight before use. Solution A was 3 % beta-alanine, 45 % water, and 52 % isopropanol. The solutions were prepared by mixing the beta-alanine with isopropanol and water mixture followed by sonication until the solution became homogeneous. Solution B only consisted of isopropanol. All the concentration ratios are by weight percent unless indicated otherwise.

For one of the experiments in Chapter 5, a synthetic chemical, 2,5-Bis(2-(4-pyridyl)-vinylene) hydroquinone dineopentyl ether (Np-P4VB) was prepared by following the protocol reported in literature[98]. The solution of Np-P4VB was prepared similarly as the alanine solution. The solvent ratio for solution A consisted of 15:4:0.35 (ethanol:water:mesitylene) with approximately 0.01 g of Np-P4VB per 50 mL of the solvents. The small amount of mesitylene (Sigma-Aldrich, 98 %) was added to minimize the use of the solute as Np-P4VB was artificially created in a small quantity. The prepared solution was then stored away from the light as the solute is sensitive to the light.

## 3.3 Procedure of oiling-out crystallization by solvent exchange

The process of solvent exchange started with solution A being filled in the flow cell as shown in Figure 3.1 (a). Solution A was then displaced by solution B at a controlled flow rate with the use of a syringe pump. The flow of solution B continued until all droplet crystallized and ran for 1-2 minutes more to get rid of possible incompleteness of droplet crystallization. The syringes and flow cell were subjected to washing by ethanol and water followed by sonication in solvents and water for 10-20 minutes

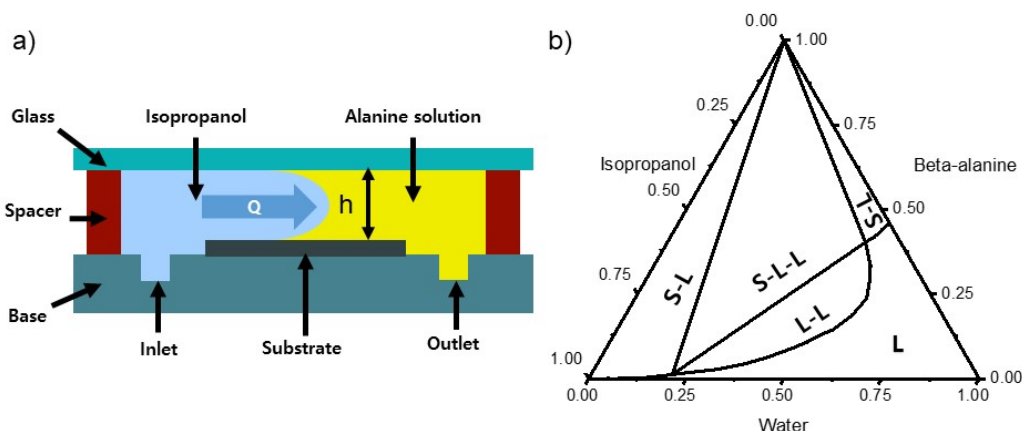


Figure 3.1: a) Sketch of the side view of fluid chamber. The solvent exchange process is progressed as alanine solution is replaced by isopropanol. b) Ternary phase diagram of beta-alanine, isopropanol, and water at 25 °C taken from Sun et al.[21] Regions on the diagram are solid-liquid region (S-L), solid-liquid-liquid region (S-L-L), liquid-liquid region (L-L), and homogeneous liquid region (L).

to avoid possible contamination or crystal leftover after each experiments. After sonication, the flow cell and syringes were dried by compressed air before assembling the flow cell for next experiment. For the adjustment of the channel height ( $h$ ), layers of double sided tape were used to create a higher platform for the substrate to reach from 100  $\mu\text{m}$  to 300  $\mu\text{m}$ .

The ternary phase diagram is referenced in Figure 3.1 (b). There are five regions within the ternary phase diagram (beta-alanine, water, and isopropanol): solid-liquid region (solute lean), solid-liquid-liquid region, solid-liquid region (solute rich), liquid-liquid region, and homogeneous liquid region, respectively. The data for the phase diagram was acquired from beta-alanine experimental works from Sun et al.[21]

### 3.4 Conditions for solvent exchange: solute concentration, flow rate, and channel height

The conditions for the main experiment can be viewed in Table 3.1 for Chapter 4 and Table 3.2 for Chapter 5.

No.	Solution A	Flow rate	Peclet number
1	3 % alanine	6 mL/hr	130
2	3 % alanine	12 mL/hr	260
3	3 % alanine	24 mL/hr	510
4	3 % alanine	50 mL/hr	1100
5	3 % alanine	70 mL/hr	1500
6	3 % alanine	110 mL/hr	2400
7	3 % alanine	200 mL/hr	4300
8	1.5 % alanine	6 mL/hr	130
9	1.5 % alanine	12 mL/hr	260

Peclet number ( $Pe$ ) is defined as  $\frac{Q}{wD}$  where  $Q$  is the flow rate,  $w$  is the channel width, and  $D$  is the diffusion constant.

Table 3.1: List of experimental conditions on homogeneous surfaces (Chapter 4)

The substrate dimension is different between the experiments in Chapter 4 (1.3 cm X 2 cm) and Chapter 5 (1 cm X 2 cm). The width of the substrate was reduced for Chapter 5 as the experiment involved the use of patterned substrate which requires more preparation time. Therefore, there are slight differences in the  $Pe$  number for the experiments between Chapter 4 and Chapter 5.

No.	Solution A	Flow rate	channel height	Peclet number
1	1.5 % alanine	6 mL/hr	300 $\mu\text{m}$	170
2	1.8 % alanine	6 mL/hr	300 $\mu\text{m}$	170
3	3 % alanine	6 mL/hr	300 $\mu\text{m}$	170
4	3 % alanine	12 mL/hr	300 $\mu\text{m}$	330
5	3 % alanine	50 mL/hr	300 $\mu\text{m}$	1400
6	3 % alanine	70 mL/hr	300 $\mu\text{m}$	1900
7	3 % alanine	70 mL/hr	200 $\mu\text{m}$	1900
8	3 % alanine	70 mL/hr	100 $\mu\text{m}$	1900

Table 3.2: List of experimental conditions on micro-patterned surfaces (Chapter 5)

### 3.5 Crystallization in bulk mixture triggered by seeds

A suspension containing crystal seeds in isopropanol in Chapter 4 was made by following process: alanine was collected from the surface after oiling-out crystallization through solvent exchange. 0.1 g of alanine was added into 50 mL isopropanol and the mixture was sonicated for 10 min until the solution turned milky. Then 0.1 mL of the milky suspension was taken out and diluted by 4 mL of isopropanol to obtain the seed suspension with the concentration of alanine particles at  $\sim 5 \times 10^{-5} g/mL$ . The collected crystals from the surface were used to trigger the bulk crystallization; an aqueous solution of alanine was prepared by dissolving 13.2 g of alanine in 17.6 mL of water. Then the solution was separated equally into two vials. 4 mL isopropanol was added into the ternary solution in one vial that was kept still for crystallization to occur. In the second vial, 4 mL of seeding suspension was added into the solution to trigger crystallization.

### 3.6 Data collection and image analysis

The videos and images for the progress of the oiling-out crystallization in the flow cell during the solvent exchange was accomplished by NIKON Eclipse Ni microscope with X-Cite Series 120 Q mercury light source. The NIKON software has a function of auto-whiting which corrects the color saturation of the videos and a function of auto-exposure correction which adjusts the brightness of the video and images. Both of these features were utilized for our experiments. For the droplet size analysis, ImageJ software was used to edit the images and collect data. The images were subjected to auto-threshold feature with "Li filter" and when the data was not clear, the threshold was adjusted manually from the auto-corrected images. The setting for threshold was important because the size recorded of the droplets in detection could be altered depending on how the image was binarized. Therefore, both the actual

droplet size and the surface coverage were larger than the recorded data. This was done for ImageJ software to be able to identify individual droplets. If not, the filter for circularity disregarded the droplets that were in contact with each other (which majority of droplets were in contact with each other).

### 3.7 Chemical and structural identification

A multipurpose X-ray (Cu-source) diffraction system Rigaku Ultima IV (nanoFAB, Edmonton, CA) was used for powder diffraction and thin film diffraction scattering. This XRD has both parallel beam (for thin film) and focus beam (for powder) slit, the detector is scintillation counter with monochromator. The scan speed was 2 °/min ranging from 10 ° to 70 ° at scan axis of  $2\theta$  with sampling width of 0.05 ° at a continuous scan mode. The beta-alanine (ACROS organics, 99%) was grounded up into fine powder and measured in powder XRD setting. The air dried crystal on the substrate after the solvent exchange was taken as the sample and measured in thin film XRD setting.

For Fourier transform infrared (FTIR), Agilent Cary 620 was used. The beta-alanine (ACROS organics, 99%) was grounded up into fine powder and the absorption of FTIR was measured. The crystal product from the solvent exchange was scraped off from the substrate after air-drying and were measured similarly.

## Chapter 4

# Oiling-out crystallization of beta-alanine on homogeneous surfaces controlled by solvent exchange

### 4.1 Results and discussion

#### 4.1.1 General trends for oiling-out crystallization through solvent exchange

The steps to oiling-out crystallization can be sub-divided into liquid-liquid phase separation (LLPS) and crystallization. During the solvent exchange, the alanine-rich aqueous phase nucleated and grew on the substrate as the mixing fronts progressed through the flow cell as described in Figure 3.1. At the start of the liquid-liquid phase separation, numerous small droplets experienced rapid droplet growth with rapid coalescence as shown in figure 4.1. As droplets coalesced to larger sizes, the droplet growth slowed down until the droplet stopped growing. The seed crystal in the bulk flow landed randomly on the substrate and the crystals would be in contact with the surface droplets. The crystals continuously grew by consuming the droplet in the surrounding. Once there were no droplets in the vicinity, the crystallization would come to a halt.

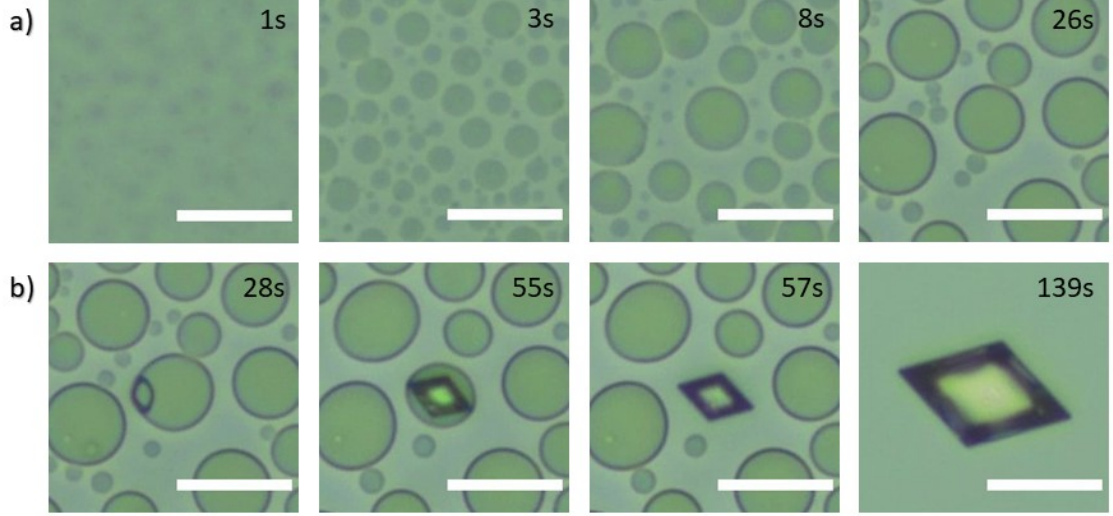


Figure 4.1: Progress of droplet nucleation and crystallization of alanine on the  $SiO_2$  substrate for condition No. 2 in Table 3.1. a) Droplet nucleation and growth. The progress from the initial nucleation to end of droplet growth. b) Crystallization in surface droplets. The progress from the initial landing of crystal seed to the consumption of the droplet which the crystal resides in. The image ends with complete consumption of neighbouring droplets to achieve final size of the crystal. Length of the scale bar: 25  $\mu m$

#### 4.1.2 Liquid-liquid phase separation by solvent exchange and droplet characterization

##### a. Estimation of the supersaturation level based on the growth rate of the droplets

LLPS during solvent exchange is driven by the solubility difference between solution A (good solvent) and solution B (poor solvent). Another way to describe the driving force is the supersaturation level between the two phases. By observing the growth of surface droplet, supersaturation level can be estimated by equation 4.1[56].

$$\frac{dM}{dt} = \pi R D \cdot (C_\infty - C_s) \cdot f(\theta) \quad (4.1)$$

The  $M$  is the total mass of the droplet,  $R$  is the radius of the surface area covered by the droplet on the substrate,  $D$  is diffusion constant,  $\theta$  is the contact angle of the

droplet on the substrate, and  $C_\infty$  and  $C_s$  are the solute concentration at the bulk and the saturation concentration in the droplet. function  $f(\theta)$  and  $g(\theta)$  is the geometric function[56].

The droplet radius is not constant with time so further simplification leads to equation 4.2 which allows correlation between concentration difference to the droplet radius and the droplet radius growth rate ( $\Delta C \propto R(t) \cdot \frac{dR}{dt}$ ). The  $k$  is a constant where  $\frac{3\rho}{D} \cdot \frac{g(\theta)}{f(\theta)}$ .

$$\Delta C = \frac{3\rho}{D} \cdot \frac{g(\theta)}{f(\theta)} \cdot R(t) \frac{dR}{dt} = k \cdot R(t) \frac{dR}{dt} \quad (4.2)$$

## b. Droplet growth analysis

Defining  $t_0$  to be at the start of the droplet nucleation on the substrate, the following progression of the droplet growth was observed by the optical microscope. As Equation 4.2 only applies for diffusion dominated droplet dynamics, following equation was applied when droplet grew without coalescence up to the appearances of the crystals in the view of the microscope. A modal sized droplet at a flow rate was selected to be analyzed. The radius of a single droplet was followed and plotted against time as shown in Figure 4.2. The following data was then plotted as  $R \cdot \frac{dR}{dt}$  to see the supersaturation level during the LLPS.

The plots in Figure 4.2 indicated the droplet growth rapidly occurred in a short time window. The droplet radius plateaued in the early stages of droplet formation therefore the corresponding supersaturation is high only in the beginning. This behaviour is different from the oil droplet growth by using an Ouzo solution[47]. For the oil droplet formation through the solvent exchange, the droplet growth occurred during the entire period of solvent exchange process. The continuous growth was attributed to the  $S_{droplet}$  from the composition in a metastable Ouzo region[47]. The short growth time for oiling-out droplets may be attributed to the lack of the

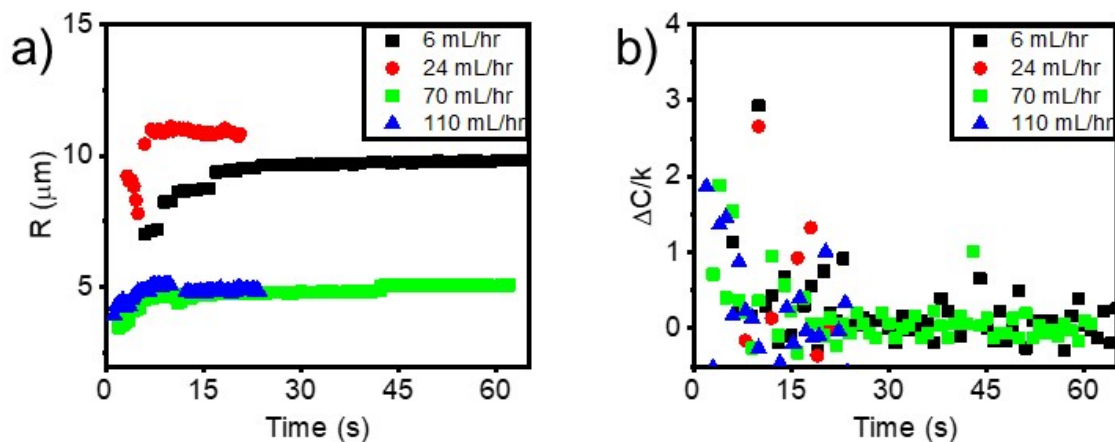


Figure 4.2: Plot of supersaturation acquired from droplet growth analysis a) Radius of a modal sized droplet at different flow rate during a diffusive droplet growth. b) Effective supersaturation level in terms of  $\Delta C/k$  at different flow rates.

metastable region in the solubility phase diagram and ternary mixture in the droplet. The composition of the droplet during the droplet formation is beyond the solubility boundary. The composition of the droplet would change with continuing solvent exchange and lead to crystallization which would be further discussed in Section 4.1.3 and 4.1.5.

In figure 4.3 (a) to (d), snapshots of droplets at different flow rates of Solution B are shown. Following droplet size distribution and droplet surface coverage was plotted as Figure 4.3 (e) and (f). Zhang et al.[30] have indicated that  $Vol_f$  final droplet volume after the solvent exchange has a correlation to a non-dimensional number  $Pe$  Peclet number as  $Vol_f \sim Pe^{3/4}$ . Therefore, the correlation showed a larger droplet size with a faster flow rate. However, no strong dependence of the droplet size with the flow rate was observed for oiling-out droplets. The surface coverage plot had the droplet occupy similarly high surface coverage for all flow rates. Both observations may be due to the short time of oiling-out droplet formation.

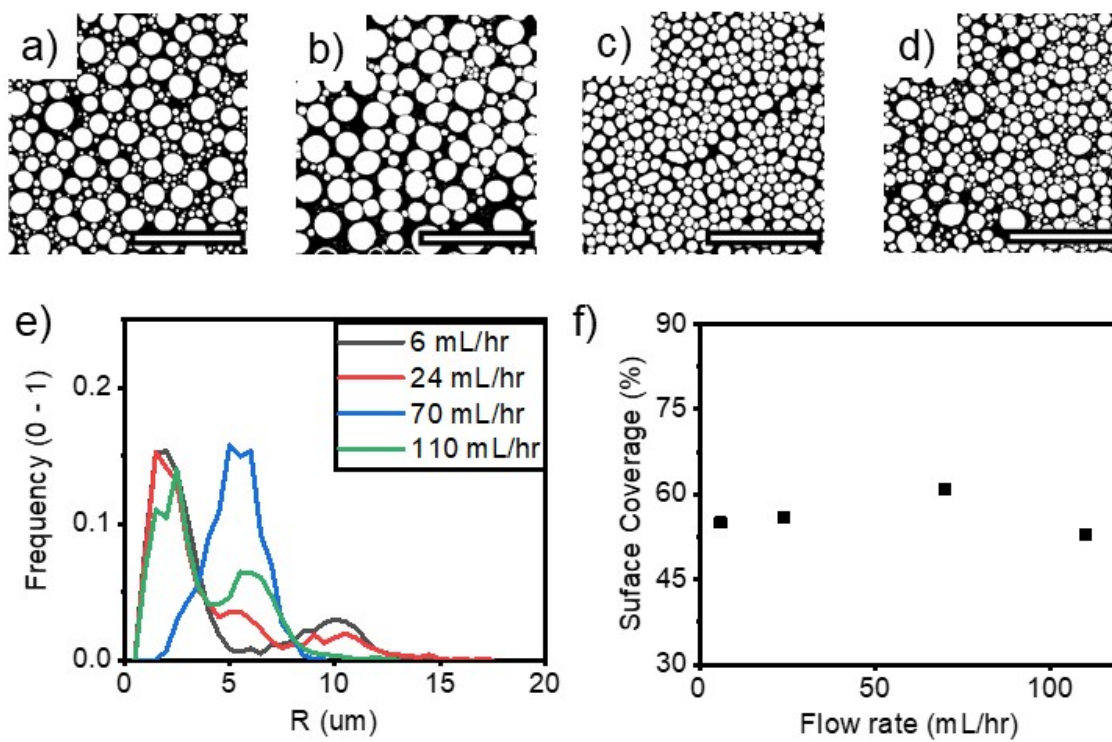


Figure 4.3: Edited image of of alanine oiling-out on  $SiO_2$  substrate during solvent exchange before crystallization with different isopropanol flow rate of a) 6 mL/hr b) 24 mL/hr c) 70 mL/hr d) 110 mL/hr. Length of the scale bar: 25  $\mu m$ . e) Plot of probability distribution function of droplet radius with varying flow rates. f) Plot of surface coverage with varying flow rates.

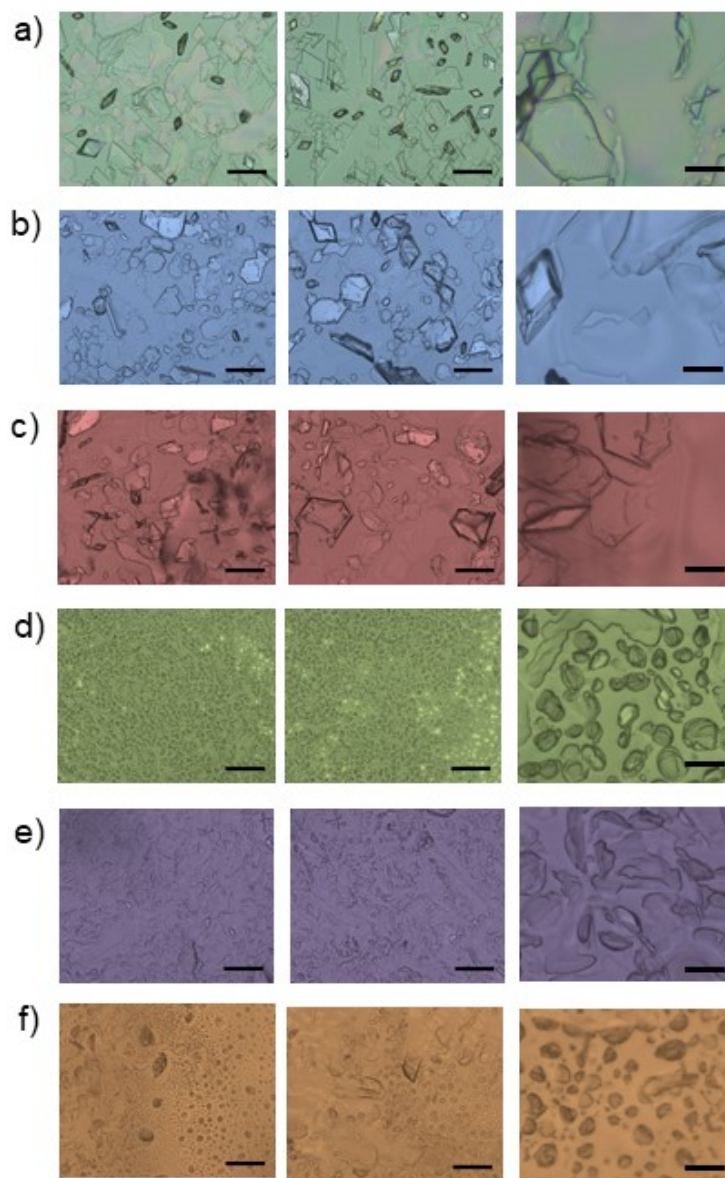


Figure 4.4: The snapshot of three separate experimental runs of alanine oiling-out crystallization on  $SiO_2$  substrate after solvent exchange that are colorized with different isopropanol flow rate of a) 6 mL/hr (Green) b) 12 mL/hr (Blue) c) 24mL/hr (Red) d) 70 mL/hr (Yellow) e) 110 mL/hr (Purple) f) 200 mL/hr (Orange). The images in first and second columns are images in their original size. Images in the third column are zoomed in images. Length of the scale bar: 100  $\mu\text{m}$  (first and second columns) and 20  $\mu\text{m}$  (third column).

### 4.1.3 Crystallization: morphology and characterization

In the observation of LLPS during oiling-out crystallization by solvent exchange, different flow rate affected the droplet size distribution. Due to the different droplet formation, crystallization that followed the LLPS caused differences in the crystal growth and its morphology. In Figure 4.4, three separate runs of solvent exchange oiling-out crystallization experiment are shown with different flow rates. The experiments showed good reproducibility with similar general features in the crystal formation. This indicated that the flow rate is one of the main parameters for controlling the crystallization through the solvent exchange. At the flow rate of 6 mL/hr to 24 mL/hr, the large amount of crystals that cover the substrate are the thin film of crystals resulting from the droplet coalescence as seen in Figure 4.4 (a) to (c). However, at a 70 mL/hr flow rate, crystals retaining the droplet shape. The droplets did not experience as much coalescence as the lower flow rates did. Faster flow rate such as 110 mL/hr to 200 mL/hr in Figure 4.4 (e) and (f), showed crystallization to be less constrained to the droplet shape.

The crystallization is triggered by the presence of the crystal landing on the substrate. In figure 4.5 (a) and (e), the droplets that are in contact with the crystal starts to form a thin layer of crystal that propagate along with the droplet coalescence (Figure 4.6). The self-propelling droplet was related to the Marangoni effect. The surface tension gradient from local crystallization caused the droplets to move toward the location of higher surface tension where the liquid had not been crystallized. The propulsion of the droplet allowed the crystallization to occur in a larger area than the base area of the precursor droplets. As the neighbouring droplets start to deplete and the crystallization is unable to propagate further, the crystallization slows down. For crystals that are relatively smaller than the droplet, the crystallization occurred by consuming the content of the droplet that the crystal is contained in as seen in figure 4.5 (b).

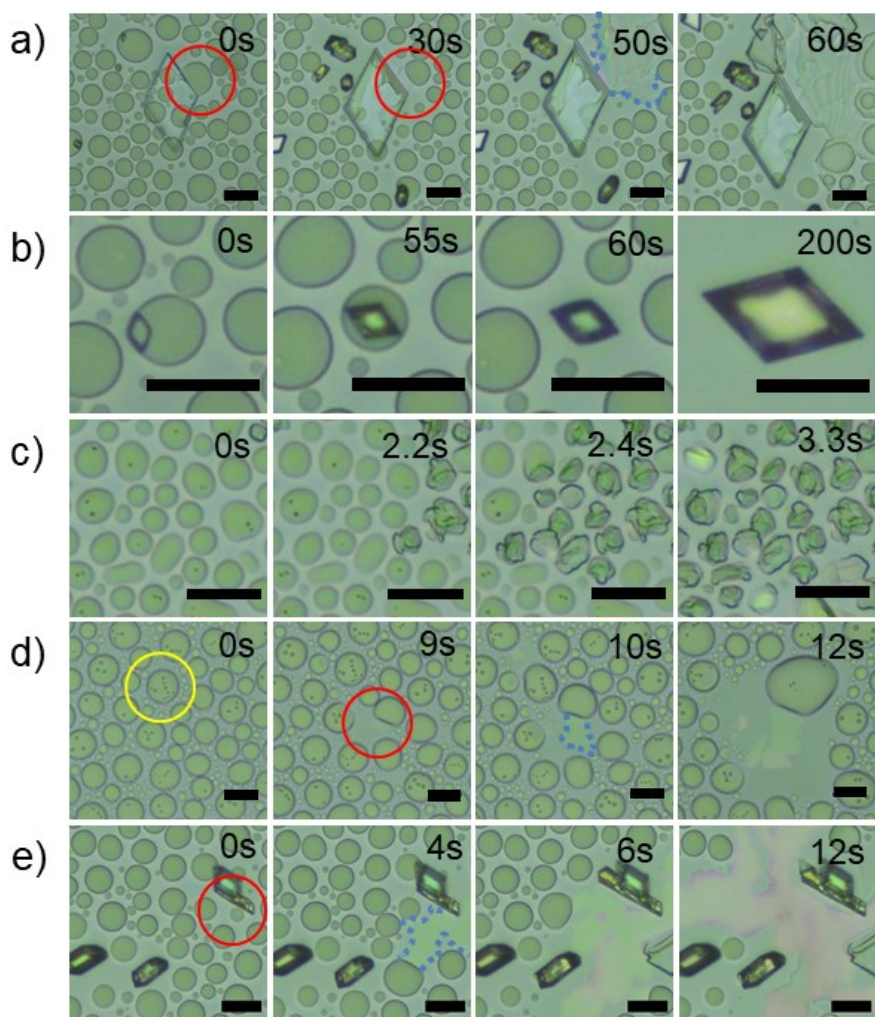


Figure 4.5: Optical microscopy of droplet crystallization triggered by droplets. a) Coalescing droplets with trail of crystals. b) crystallization within a single droplet. c) droplet crystallization triggered by droplet coalescence. d) droplet crystallization triggered by droplet coalescence. e) Thin film crystallization by droplet coalescence.  $t_0$  is defined to be the initial time of seed crystal landing on the substrate. The conditions are No. 2 for a), b), and e) and No. 5 for c) and d) in Table 3.1. The red circle indicates the initial droplet that starts to crystallize. The blue dotted line indicates the boundary of the thin film crystals. Yellow circle indicates the alanine phase encapsulated by alanine-rich phase. Length of the scale bar: 25  $\mu\text{m}$ .

In the special case of 70 mL/hr, the crystallization progressed in cascading fashion where the droplets in the vicinity of the newly formed crystal would crystallize first. Similar occurrence was observed in the works of Abramov et al[99]. During the cooling of a solution of hexadecane oil in water with a surfactant, “different to crystallization at low supercooling, at higher supercooling droplet tended to crystallize in the neighborhood of already solidified droplets.” In our experiment, we believe that the cascading crystallization is due to the combination of high supersaturation level in the droplet with an uniform of droplet size distribution for 70 mL/hr of flow rate. The processes for the thin film crystallization and the non-coalescing droplet crystallization are outlined in the figure 4.6. For the observation of crystallization, we define  $t_0$  to be the initial time of the seed crystal landing on the substrate as shown in figure 4.5 and 4.7

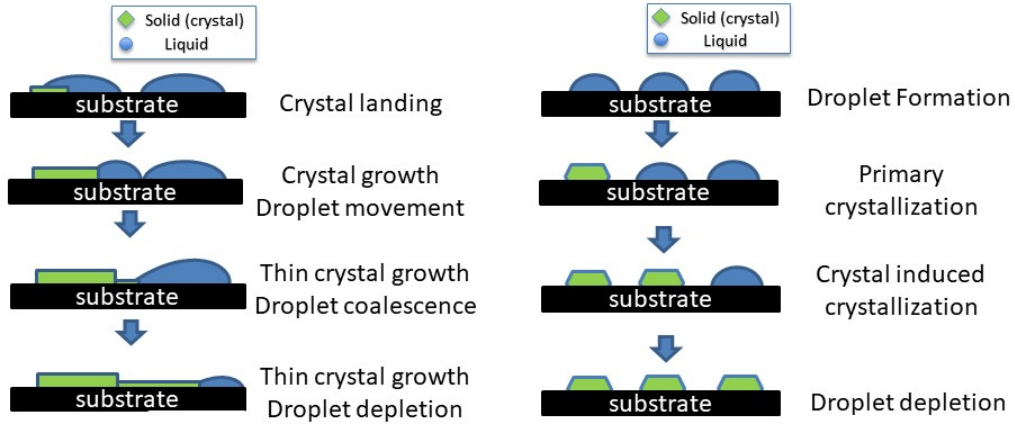


Figure 4.6: Diagram of thin film crystal growth by droplet coalescence and without droplet coalescence (unique to 70 mL/hr flow rate).

The orientation of the crystals that landed on the substrate has significant effect on how the crystal growth occurred. Three common morphology of crystals was observed during the solvent exchange namely polygonal shape, needle-like shape, and diamond shape. Figure 4.7 (a) shows crystal growing in a polygonal shape as the crystals

consumed the content in the droplet. Figure 4.7 (b) showed crystal extending in only one direction to form a long needle-like crystal. In certain cases, the crystal may extend in both direction. Figure 4.7 (c) shows crystal growth extended in a diamond shape. Interestingly, in the works of Shanthi et al.[100], this is the shape that was observed in slow evaporation crystallization technique and are also most commonly observed shape in our experiments. The different shapes of crystals may be due to the projection of diamond shape on the plane of 2D images.

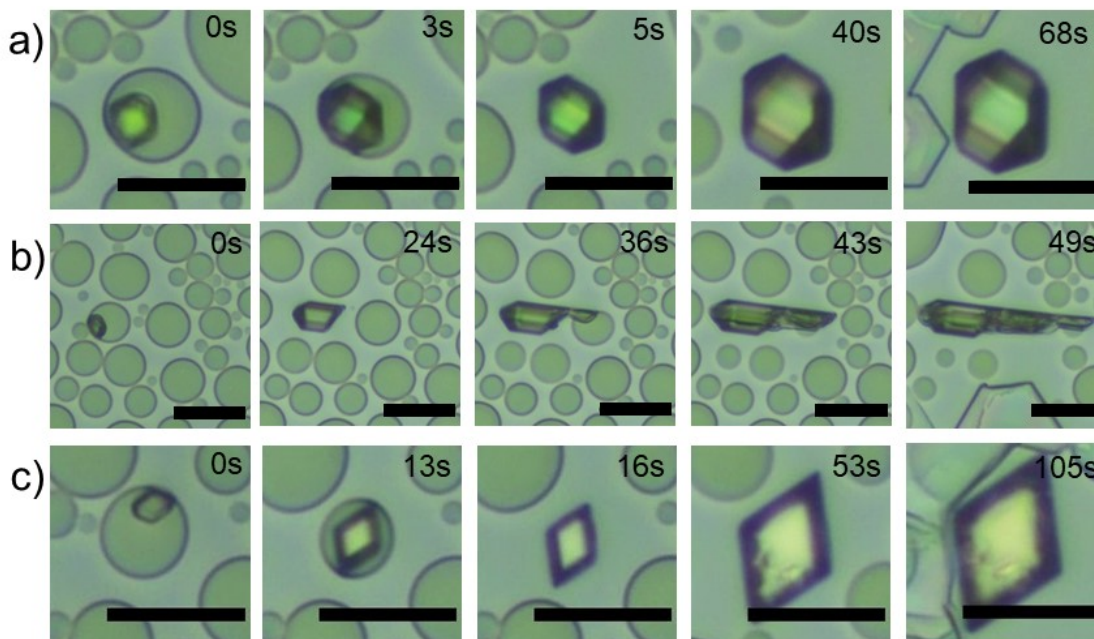


Figure 4.7: Optical microscopy of droplet crystallization of different crystal morphology caused by facet effect. The crystals shapes were a) polygonal shape b) needle-like shape c) diamond shape. Scale bar: 25  $\mu\text{m}$ . The condition for solvent exchange is listed as No. 2 in Table 3.1.

The crystal growth rate was analyzed by tracking the area occupied by the selected crystals as shown in the figure 4.8. The selected crystals are shown in figure 4.8 for (a) 6 mL/hr and (b) 12 mL/hr. The plots on figure 4.8 (c) and (d) shows that crystal growth rate does increase with flow rate. At 6 mL/hr flow rate, the crystal growth rate was slow for initial  $\sim 25\text{s}$  and the rate increased for the next 10s or so. The sharp increase in the growth rate may be related to a high supersaturation level by

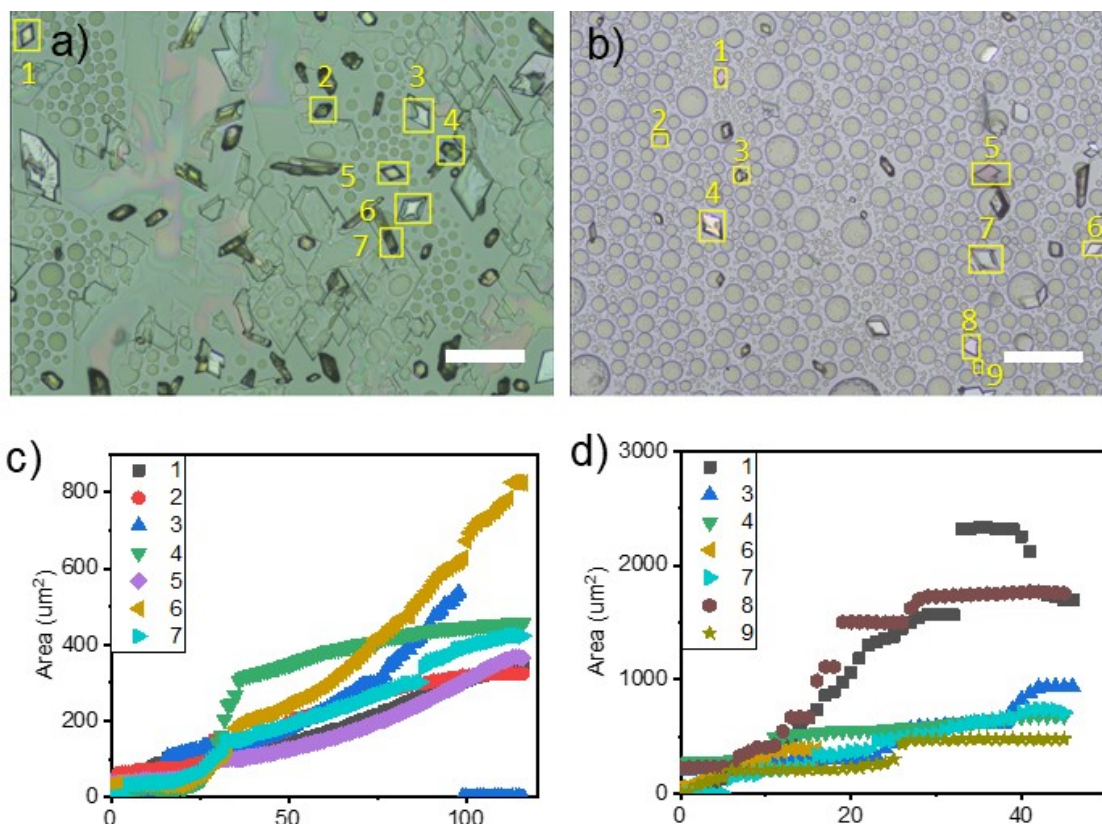


Figure 4.8: Optical microscopy during oiling-out crystallization on  $SiO_2$  substrate with crystals numbered for growth analysis a) for 6 mL/hr b) for 12 mL/hr. The plot of area of the crystal observed on microscope versus time for the numbered crystals c) for 6 mL/hr d) 12 mL/hr. Scale bar: 100  $\mu m$ .

the solvent exchange method.

#### 4.1.4 Effect of surface wettability

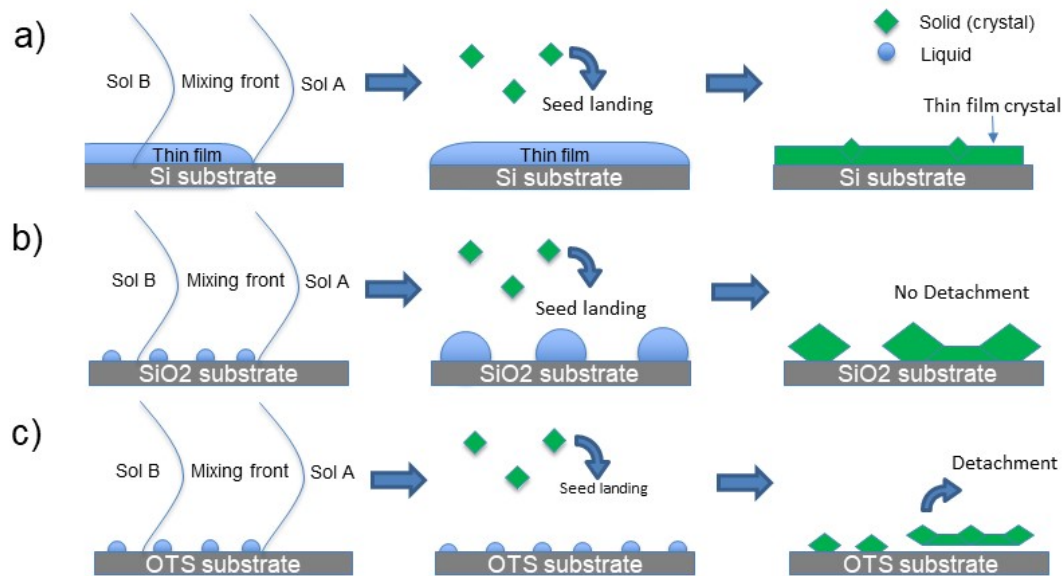


Figure 4.9: Diagram of general trend for alanine oiling-out crystallization on different substrate surfaces. Liquid-liquid phase separation and crystallization a) on bare silicon b) on  $SiO_2$  c) on OTS coated bare silicon.

For each substrate with different wettability, the behaviour of liquid-liquid phase separation and crystallization were different. For bare silicon, the nucleated liquid spread on the substrate and was observed to form a thin film of liquid on top of the substrate as described by figure 4.9 (a). The thin film of crystal preferred to spread on the substrate as the high surface energy leads to crystal formation favouring along the substrate. Eventually, the alanine-rich liquid phase would be all consumed by the crystallization or dissolution to the bulk flow. The observed phenomenon can be seen in figure 4.10 (a).

For  $SiO_2$  substrate, the droplets were pinned to the substrate and grew by coalescence as described in Figure 4.9 (b). The crystallization continued until all the droplets were consumed as described in figure 4.10 (b). Some droplet may coalesce

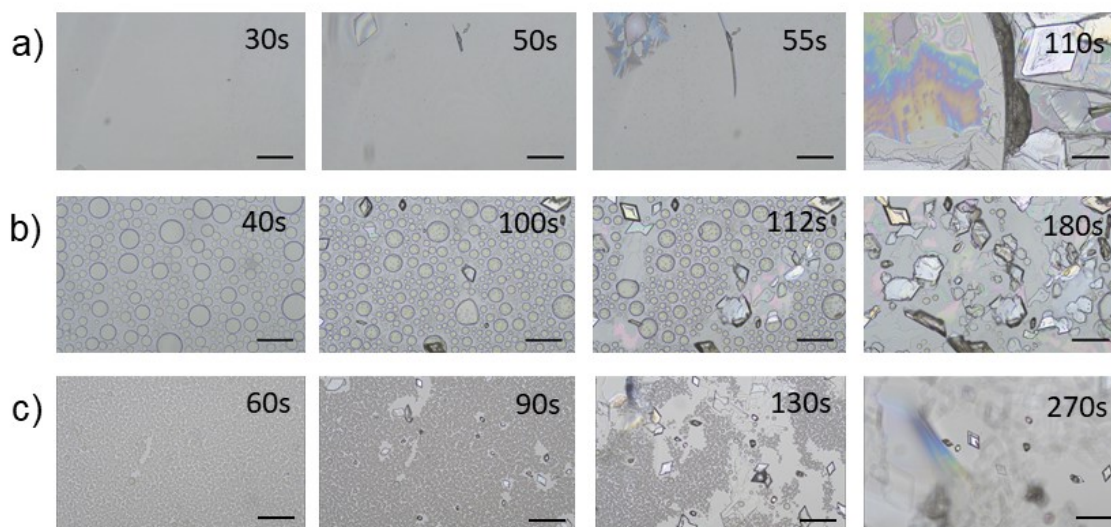


Figure 4.10: Optical microscope images of general trend for alanine oiling-out crystallization on different substrate. Liquid-liquid phase separation and crystallization a) on bare silicon, b) on  $SiO_2$ , and c) on OTS coated bare silicon. The conditions for solvent exchange is No. 2 in Table 3.1.  $t_0$  was set to the initial observation of droplet nucleation on the substrate. Scale bar: 100  $\mu m$ .

during the crystallization and lead to having irregular shaped crystals as described in the previous sections.

For hydrophobic OTS-coated silicon substrate, solute rich aqueous phase was pinned to the surface during the solvent exchange as described in figure 4.9 (c). The droplets then proceeded to grow and coalesced on the substrate until crystallization is triggered. However, droplets did not grow as large as seen in  $SiO_2$  experiments and the droplets coalesced for a relatively small amount (figure 4.10). The droplet nucleation on a hydrophobic surface is not favourable for alanine oiling-out crystallization as evident from a small amount of droplet nucleation.

Different to oiling-out crystallization on  $SiO_2$ , crystals on OTS-coated substrate were quite easily detached and will move along with the bulk flow. The crystals were irregular in shapes as crystallization progressed with the coalesce of droplets. As the droplets continued to move, the droplets leave a thin film of crystals behind their path and formed a large irregular shape of crystals as observed in figure 4.10 (c).

The crystallization on the hydrophobic surface must not be favourable for alanine oiling-out as the crystals are easily detached from the substrate.

After the solvent exchange was completed, the structure of alanine crystals on different substrate have been characterized by infrared and X-ray diffraction measurement as shown in Figure 4.11. Regardless of which substrate was used for the solvent exchange, same peaks of XRD and IR were observed. This proved that the crystals were same polymorph as the bulk alanine crystals. There are some differences between the intensities of the XRD and IR measurement and this may be due to the different quantities, orientations, and crystal sizes of the measured crystal samples without milling.

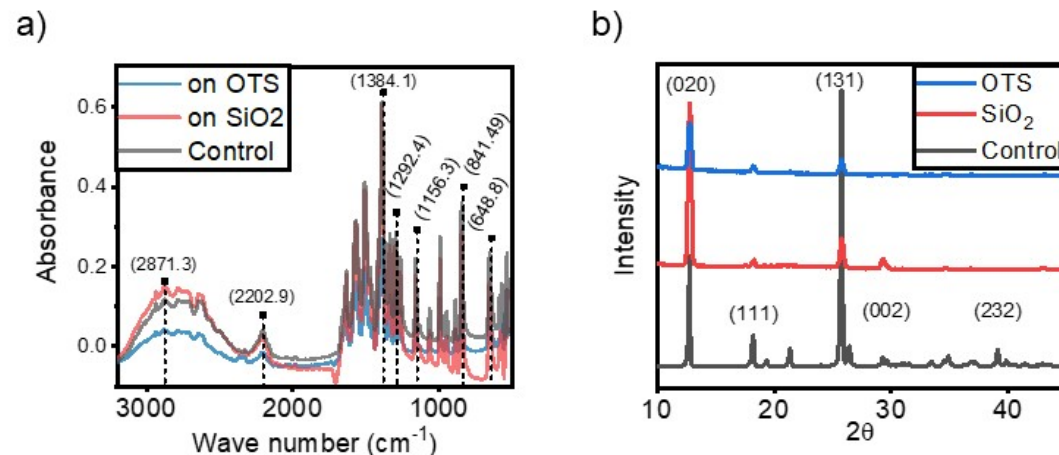


Figure 4.11: FTIR and XRD data of alanine crystals. a) Powder FTIR absorption of the collected beta-alanine crystal sample from solvent exchange. b) XRD of collected alanine crystal sample on OTS and  $SiO_2$  and the control sample of alanine. The sample for FTIR and XRD are from the condition listed as No. 2 in Table 3.1.

#### 4.1.5 Discussion

The ternary phase diagram is typically used for understanding the phase separation during solvent exchange[36]. During the solvent exchange, the oiling-out system will go through changes in composition in a path known as dilution path as indicated by the blue dotted line in Figure 4.12. When the composition enters the L-L region, the

solution separates into two phases: alanine-rich phase and alanine-lean phase. The alanine-rich phase formed droplets on the solid surface while the alanine-lean phase would be transported away by the flow of the antisolvent. the excess alanine-lean phase will form smaller droplets within the alanine-rich phase.

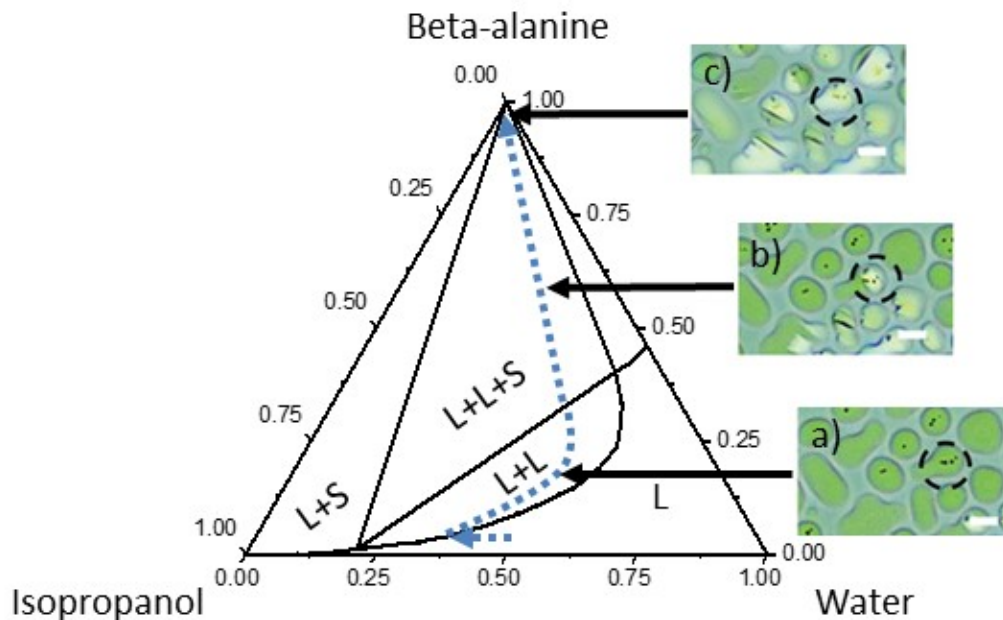


Figure 4.12: Oiling-out crystallization in the LLPS droplet inside the black dashed circle. a) Before crystallization (L-L region) with small droplets (alanine-lean) inside a big droplet (alanine-rich), b) during the crystallization (L-L-S region) with the crystals inside the droplets, c) end of crystallization (Solid phase) with all droplet consumed. The crystallization images are from the experimental condition No. 5 in Table 3.1. Length of the scale bar: 10  $\mu\text{m}$ .

The mechanism for alanine oiling-out crystallization seem to be the effect of counter diffusion[21]. Counter diffusion is a phenomenon that is utilized when forming a spherical crystals in oiling-out crystallization[19, 20]. After the formation of the droplet, the antisolvent is continuously supplied to the droplet by solvent exchange. As both the solvent and antisolvents are miscible with each other, the antisolvent diffuses into the droplet while the solvent diffuses out of the droplet. This leads to solubility of the droplet to decrease until a phase change can be triggered (Figure 4.12 (b)). In the cases for our experiments, the rate that the solvent diffuses out of

the droplet and antisolvent diffuses into the droplet is both affected by the flow rate of solution B. Therefore, the oiling-out crystallization by solvent exchange method can be controlled through different flow rates.

For all crystal growth, even if the crystals were not in direct contact to the droplet, the crystal grew by consuming the contents from neighbouring droplets. The droplets around the crystals dissolved and depleted quicker than the droplets that were further away from the crystals. This process was attributed to the diffusive interaction between the droplets and the growing crystals. The energy required for crystal growth is considered to be negligible in comparison to the crystal nucleation.[69] Therefore, the solute in the droplet would favour incorporation into the crystal rather than nucleating new crystals in the droplet. The resulting mechanism is the same as Ostwald ripening in the minimization of the free energy.

#### 4.1.6 Solution crystallization in liquid-liquid phase separated solution triggered by the seed crystals

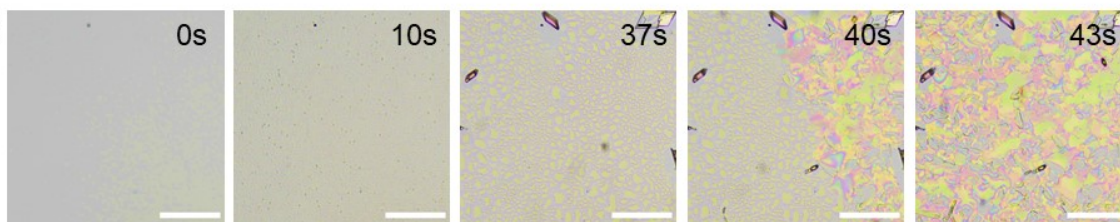


Figure 4.13: Optical microscopy of alanine oiling-out crystallization on SiO<sub>2</sub> substrate after solvent exchange by using lower concentration of alanine (1.5 %) in solution A. The condition for solvent exchange is No. 9 in Table 3.1. Scale bar: 100  $\mu$ m)

As both solvent exchange process and crystallization process were affected by the initial concentration of the solute in the solution, the oiling-out crystallization was tested with a lower concentration of alanine in solution A. Solution A of 1.5 % of alanine in water and isopropanol mixture, was used instead of 3 % shown in the previous figures. In figure 4.13 shows that lowering the initial concentration caused more thin film crystals to form. This is probably due to combination of relatively small

droplets formed during the liquid-liquid phase separation and less crystals formed in the bulk flow. Crystallization in a lower alanine concentration was achievable by the solvent exchange method while the bulk crystallization would have difficulty in triggering the crystallization.

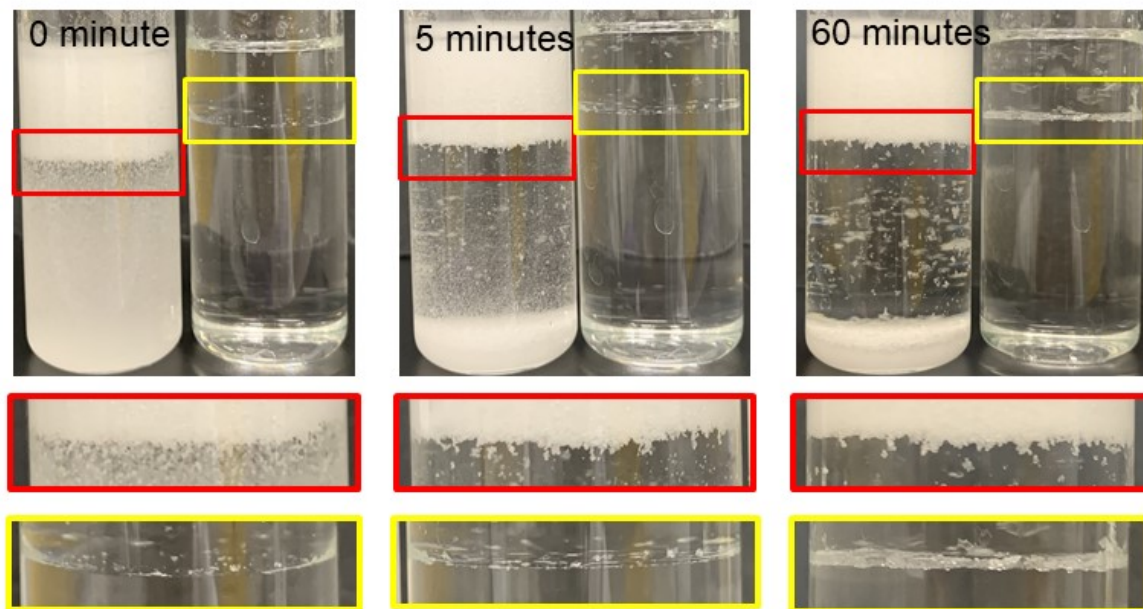


Figure 4.14: Crystallization in bulk solution with (left) and without (right) seeds. The interface between two liquid phases is shown in the two images on the bottom as with (red) and without (yellow) seeds.

To test the crystal seed from the low alanine solvent exchange crystallization, two solution, where one resembled a bulk crystallization and another resembled a seeded crystallization, was created (Figure 4.14). The bulk crystallization solution was created in the S-L-L region of the ternary diagram for alanine, water, and isopropanol. The mass ratio for the solution were 6.6 (alanine), 8.8 (water), and 5.1 (Isopropanol). Immediately upon mixing, the solution separated to two liquid phase with a small amount of crystals formed at the interface of the liquid phases. As more time passed, the formation of crystals at the interface continued. For the case with the crystal seeds, the two liquid phases from the solution was mixed with crystal seeds ( $5 \times 10^{-5}g/mL$ ). Immediately, the solution became milky and a large amount

of crystals formed. The results demonstrated that the oiling-out crystallization by solvent exchange may be used to produce crystal at a low concentration that can be used to trigger phase separation in the bulk mixture.

## 4.2 Conclusion

The literature lacked in using solvent exchange to study system with oiling-out crystallization phenomenon. We demonstrated that using flow rate, initial concentration of solution A, and surface wettability for the solvent exchange can provide control and understanding to the phenomenon of oiling-out crystallization. The main features in the droplet formation and crystallization were observed through the optical microscope and were reproducible in our experiments. The droplet formation and the morphology of the crystal changed with the flow rate and surface wettability. The droplet growth had shorter time window for faster flow rate due to the increase of diffusion of the solvents in the droplet. We demonstrated that a thin film of crystal or a network of irregular crystals can be formed in the path of droplet coalescence. Particularly for 70 mL/hr flow rate, the crystals were constrained by the droplets and crystallized in the location of the droplet. Solvent exchange showed crystallization even at very low solute concentration, which cannot be easily achieved in bulk crystallization. The collected crystals obtained from the low solute condition were able to trigger crystallization in the bulk solution, showing potential use of solvent exchange method for seed crystal formation.

The results in the study shows great advantages of using solvent exchange for system with oiling-out crystallization phenomenon. Further studies in other chemicals, conditions, and parameters that may effect the oiling-out crystallization is still need to form more complete understanding on the topic of oiling-out crystallization by solvent exchange. Our hope is that this study can start the development of oiling-out crystallization mechanism by solvent exchange flow cell that may be valuable for controlling the oiling-out in the processes, separation, and purification of crystals or

even functional surfaces, pharmaceutical development, and many other application.

# Chapter 5

## Effects of chemical and geometric micro-structures on crystallization of surface droplets during solvent exchange

### 5.1 Results and discussion

Effects of chemical patterns on the oiling-out crystallization are coupled with the influences from other conditions including hydrophobicity/hydrophilicity of the micro-patterns, flow rate, channel geometry, and solute concentration. We will show effects from chemical micro-patterns on smooth surfaces. Oiling-out crystallization on micro-structured surfaces and then from geometrical structures of micro-lenses and an inserted bubble. Finally, we will demonstrate that solvent exchange can be used to induce crystallization of a solute other than alanine.

#### 5.1.1 Oiling-out crystallization on surfaces with chemical micro-patterns

##### a. Hydrophobic or hydrophilic micro-patterns

During the solvent exchange at a flow rate of 12 mL/hr, a thin layer of liquid formed in the hydrophilic surrounding area while some small droplets formed on the hydrophobic micro-patterns as shown in Figure 5.1 (a)(b). The crystals evolved to a needle-like shape or a thin film similar to crystallization on homogeneous hydrophilic surfaces by

solvent exchange[26]. In the cases where the crystallization of a thin film occurred, small holes formed at the locations where the hydrophobic domains lied.

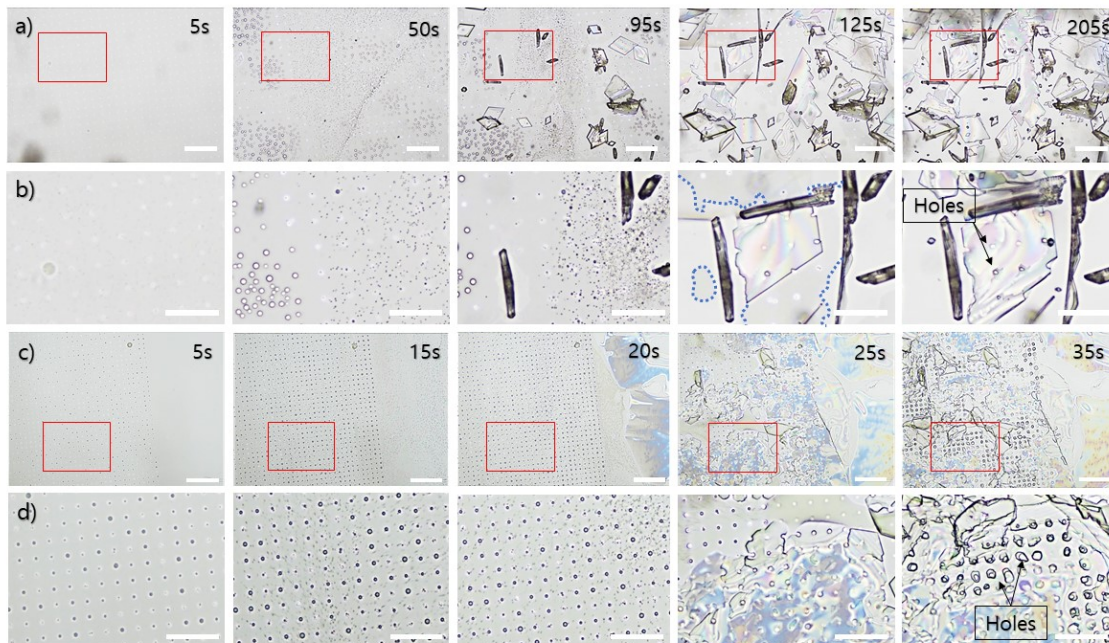


Figure 5.1: Oiling-out crystallization on the hydrophobic patterned substrate. a) At 12 mL/hr flow rate, b) the zoomed in images of the red highlighted square in a). The blue dotted line indicates the boundary of thin liquid film. c) At 70 mL/hr flow rate, d) the zoomed in images of the red highlighted square in c). Channel height: 300  $\mu\text{m}$ . Length of the scale bar: a) and c) 100  $\mu\text{m}$  and b) and d) 50  $\mu\text{m}$ .

At a faster flow rate of 70 mL/hr, droplets formed a regular array, and the holes became more apparent where the thin crystal film propagated along the surface (Figure 5.1 (c)(d)). The position of holes copied the arrangement of patterns. Peng et al.[40, 59] showed that the formation of droplets could be controlled by the patterned substrate due to preferential nucleation of oil droplets on hydrophobic areas. The alanine-rich sub-phase from oiling-out appeared to spread on the hydrophilic areas but not on the hydrophobic domains; therefore, the local rupture of the film led to the hole formation on the crystal film. This result suggested that we may make different hole arrangements on the crystal film by changing the pattern position. In particular, the size of crystal film is large at a faster flow rate, and the hole array is more regular. Such holes may allow gases, chemicals, or particles to permeate through the film.

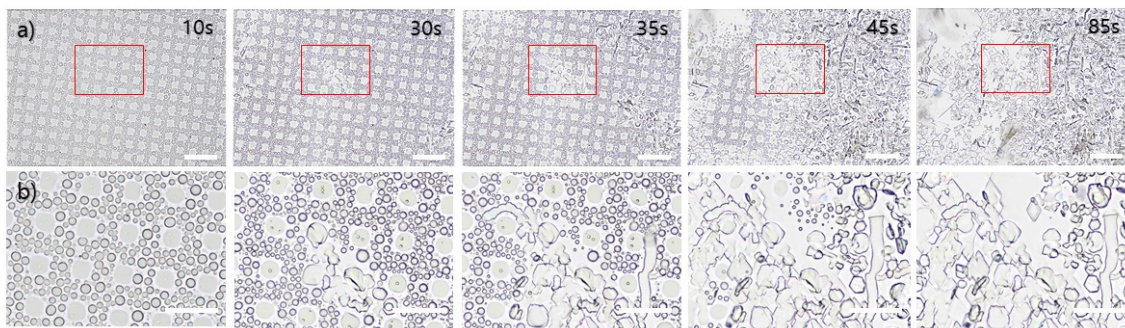


Figure 5.2: Oiling-out crystallization on the patterned substrates. a) on hydrophilic micro-patterns b) the zoomed in images of the red highlighted square in a). Length of the scale bar: a) 100  $\mu\text{m}$  and b) 50  $\mu\text{m}$ . The condition for solvent exchange is listed as No. 6 in Table 3.2.

The oiling-out crystallization behaviour on the substrate with hydrophilic pattern and hydrophobic background is shown in Figure 5.2 (a)(b). The droplets in hydrophilic domains are large with uniform droplet size, possibly due to the constraints from the patterns on the surface. Smaller droplets nucleated on the hydrophobic surrounding area with less uniform size distribution. The crystallization process propagated in the path of the droplet coalescence. The crystals are irregularly shaped, and the network of crystals is related to the hydrophilic patterns. The time from the initial crystallization to completion of crystallization in the field of view is around 50 s, almost twice the time on hydrophobic patterns in Figure 5.1 (a)(b). A longer time for the crystal growth may be due to more droplets on the surface going through phase separation, requiring more solvent supplied from the flow.

At a slower flow rate of 6 mL/hr in Figure 5.3 (b), the hydrophilic patterns on the substrate had an even clearer effect on the droplet formation and crystallization. The position and shape of the droplets follow the pattern of the hydrophilic domains on the surface which in turn led to numerous and smaller crystals. In contrast, on a homogeneous APTES-coated substrate, the size of the crystals was much larger on average. Further studies on pattern sizes or different chemical patterns may allow optimization of solvent exchange for a specific crystal morphology and pattern.

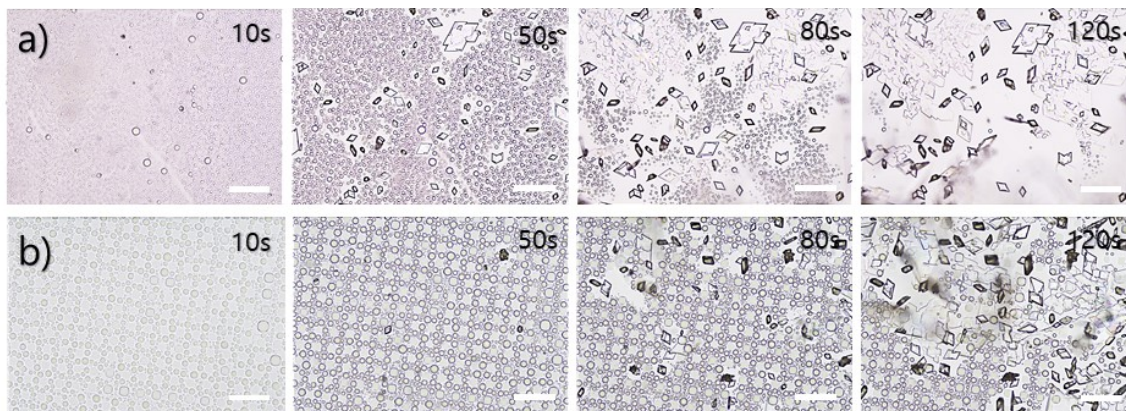


Figure 5.3: Oiling-out crystallization of droplets on a) homogeneous surface, b) hydrophilic patterns and hydrophobic surrounding area. Length of the scale bar: 100  $\mu\text{m}$ . The condition for solvent exchange is listed as No. 3 in Table 3.2.

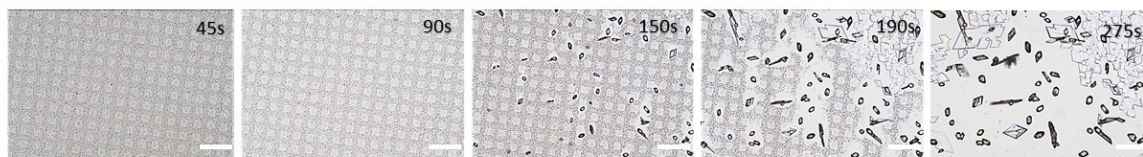


Figure 5.4: Oiling-out crystallization with the low alanine concentration. The condition for the solvent exchange is No. 2 in Table 3.2. Length of the scale bar: 100  $\mu\text{m}$ .

The initial concentration of the solute also has an important effect on the droplet formation in the solvent exchange system. At an even lower concentration at 1.8 % alanine in solution A, Figure 5.4 shows the decrease in crystals in comparison to the concentration of 3 % in Figure 5.5 (a). However, the features in the droplet formation and the crystallization are similar to each other. The main differences are the smaller surface droplet coverage and the crystallization at a lower concentration of alanine, suggesting that there is a threshold of initial concentration required for oiling-out crystallization by solvent exchange.

### b. Flow rate of the poor solvent

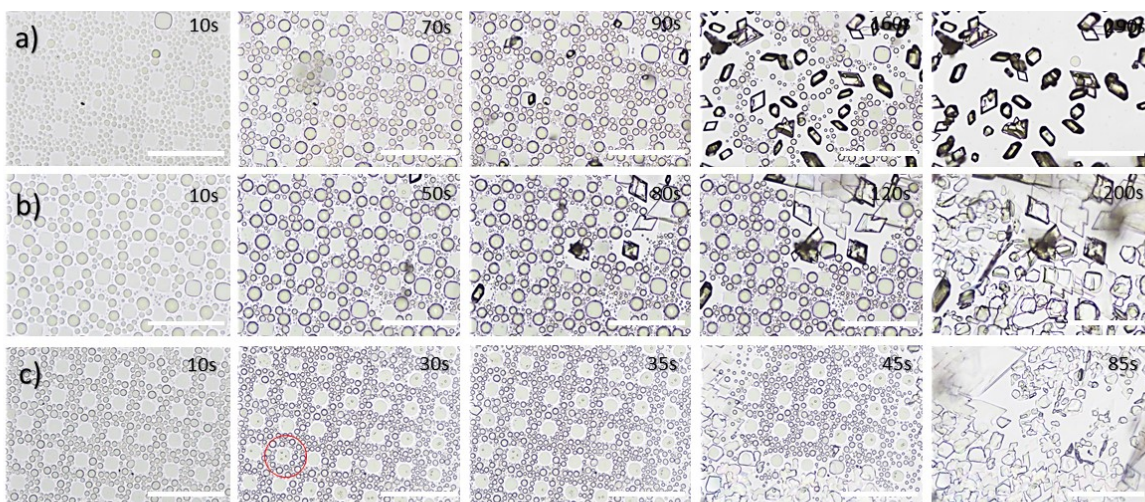


Figure 5.5: Oiling-out crystallization at the flow rate of a) 6 mL/hr, b) 12 mL/hr, and c) 70 mL/hr. The red circle indicates a case where alanine-lean droplets are encapsulated by the alanine-rich phase. Length of the scale bar: 100  $\mu\text{m}$ .

In Figure 5.5, the channel height is kept constant while the flow rate varies. The droplets at lower flow rates lasted longer before crystallization and were more likely to dissolve instead of coming to full crystallization. The completion of droplet depletion took around 290 seconds for 6 mL/hr, 200 seconds for 12 mL/hr, and 85 seconds for 70 mL/hr. All three flow rates had a single droplet that covered the hydrophilic area, suggesting that the patterns effectively controlled the droplet size regardless of the flow rate.

At the slowest flow rate of 6 mL/hr, crystals on the surface had more polygonal shapes. Some crystals may agglomerate to form clusters of crystals. For 12 mL/hr, more flat crystals grew in diamond shape while still having few polygonal shapes. At the fastest flow rate of 70 mL/hr, the droplets crystallized in a network that spreads in a radiating fashion. These crystals were more irregular in shape, and the crystallization followed the path of the droplet coalescence. Different from crystallization on homogeneous surfaces, a faster flow rate led to large quantities of crystals of the droplet shape.[26]

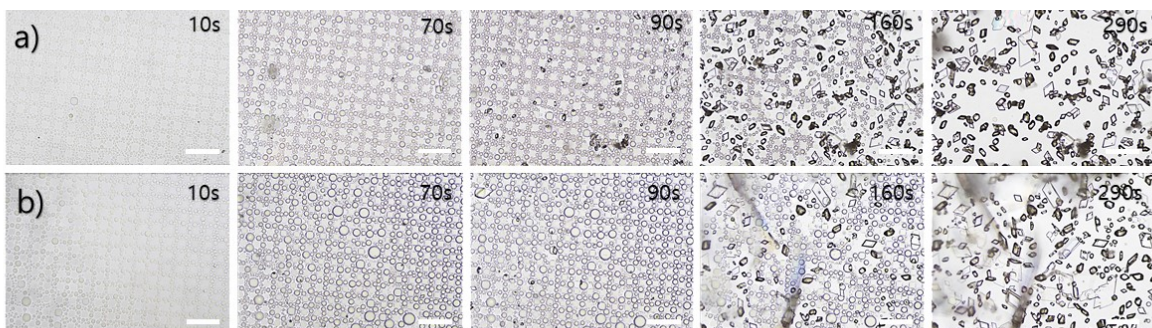


Figure 5.6: Oiling-out crystallization at the flow rate of 6 mL/hr. a) and b) are the repeats of the experiments at condition No. 3 in Table 3.2. Length of the scale bar: 100  $\mu\text{m}$ .

The general features in crystallization were reproducible under the same experimental conditions. As shown in Figure 5.6, some parts of the substrate or different experimental repeats may exhibit more flat crystal growth with diamond shapes. The crystals formed on patterned surfaces are much less polydispersed compared to those on a homogeneous surface. The number of crystals per  $\text{mm}^2$  detected by the software came out to be 391 and 401 for Figure 5.6 (a) and (b), respectively. Again, this indicated that general features of oiling-out crystallization were reproducible.

Faster crystallization at a faster flow rate of solvent exchange was explained by the transport of good solvent out from the droplets[26, 30]. In brief, water diffuses out from the droplets sooner at higher flow rates, leading to the supersaturation of alanine in the droplets in a shorter time.

The flow rate can also influence the crystallization by varying the number of the crystal seeds that land on the substrates, which is significantly greater at lower flow rates as shown in Figure 5.5 (a). More seeds led to smaller crystals at lower flow rates compared to larger connected crystals at higher flow rates. Two reasons may be at play for more crystal seeds at lower flow rates. One may be due to a later crystal landing time. The droplets in the flow experienced counter diffusion, which triggers the crystallization as observed for spherical alanine crystal formation from droplets in work by Sun et al.[23] The longer retention time for the ternary droplets in the flow may form more crystals in the flow before reaching a certain location on the substrate. Secondly, the slower flow rate allows more crystals to settle onto the surface in competition with advection by the bulk flow. Therefore, more crystal seeds can land on the substrate during the solvent exchange process.

### **c. Height of the channel for solvent exchange**

The crystallization from the solvent exchange performed in the channels with three different heights is shown in Figure 5.7. The substrates with hydrophilic micro-patterns surrounded by hydrophobic areas were used in the experiment (Figure 5.7 (a)-(c)). At a given flow rate of 70 mL/hr, the droplet size decreased with a decrease in the channel height. There was only one droplet per micro-domain at the channel height of 200  $\mu\text{m}$  or 300  $\mu\text{m}$ , but multiple droplets at the channel height of 100  $\mu\text{m}$ .

As a comparison, effects from channel height were also examined on homogeneous APTES-coated substrate (Figure 5.7 (d)(e)). Crystallization followed the droplet formation with the channel height of 200  $\mu\text{m}$  and 300  $\mu\text{m}$ . When channel height was down to 100  $\mu\text{m}$ , no droplet formation was observed. The droplets decreased in size with the decrease in channel heights. The dependence of droplet sizes on the channel height is consistent with that on the micro-patterned substrate.

The previous work showed that by solvent exchange, the final volume of the droplet  $V_f$  increased with the channel height  $h$ [30, 49]. At the same flow rate (in volume per

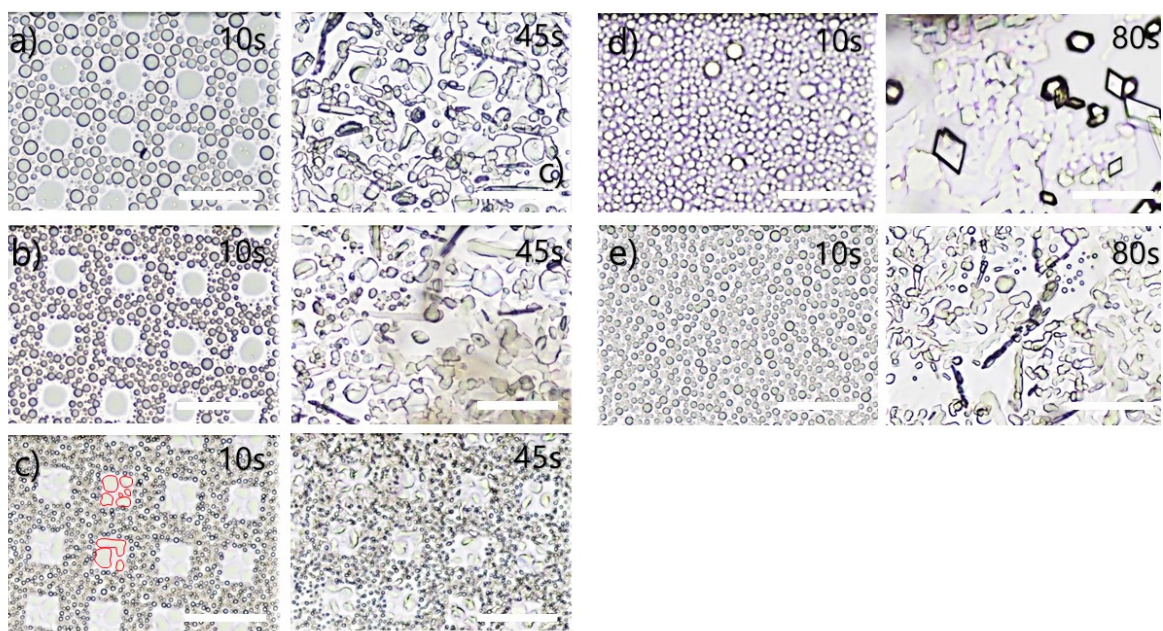


Figure 5.7: Decreasing droplet size with decrease in channel heights. Droplets and crystals on the patterned substrate at a) 300  $\mu\text{m}$ , b) 200  $\mu\text{m}$ , and c) 100  $\mu\text{m}$  and on the homogeneous substrate at channel height of d) 300  $\mu\text{m}$  and e) 200  $\mu\text{m}$ . The red outline indicates the droplet outline in the hydrophilic domain. Length of the scale bar: 50  $\mu\text{m}$ .

unit time),  $V_f \sim h^3$  because  $h$  determines how long it takes for the solution A and B to mix uniformly across the channel. The higher the channel, the longer the time for the droplets to grow [30, 49].

Above certain channel height, the effect of gravity on the mixing between two solutions may also become important. Archimedes number  $Ar$  is the dimensionless number to describe the gravity effect, arising from the density difference between solution A and the displacing solution [49].

$$Ar = \frac{g(h)^3 \Delta\rho}{\nu^2 \rho} \quad (5.1)$$

The density of the solvents in solution A is  $0.885 \text{ g/mL}$ , while solution B is  $0.786 \text{ g/mL}$ . The density difference  $\Delta \rho$  is  $\sim 0.1 \text{ g/mL}$ , the gravitational acceleration  $g$  is  $9.8 \text{ m/s}^2$ , and viscosity  $\nu$  is  $2.8 \times 10^{-6} \text{ m}^2/\text{s}$ . For our channel height  $h$  of 100, 200, and 300  $\mu\text{m}$ , the  $Ar$  number is 0.16, 1.3, and 4.3, respectively. For such a large Archimedes number ( $Ar > 1$ ) at the channel height  $h$  of 300  $\mu\text{m}$ , the center of the parabolic mixing front in the laminar flow is shifted towards the bottom surface under the gravity. Such shift would lead to a longer growth time for droplets and crystals on the top surface than on the bottom surfaces of a horizontal channel. However, the gravity effect could be eliminated by placing the channel vertically [49].

Another effect that may arise in a higher channel is enhanced mixing from convection [30, 49]. To estimate when the convection rolls set in due to the density difference, we calculate Rayleigh number  $Ra$ .

$$Ra = \frac{\Delta\rho g(h/2)^3}{\mu D} \quad (5.2)$$

where  $\mu$  is the dynamic viscosity of solution A and the mass diffusion coefficient  $D$  is approximately  $10^{-5} \text{ cm}^2/\text{s}$ . For the channel height  $h$  of 100, 200, and 300  $\mu\text{m}$ ,  $Ra$  number is 71, 570, 1900, respectively. The convection rolls may occur for 300  $\mu\text{m}$  channel heights where the Rayleigh number is slightly above the critical Rayleigh number 1708[61]. These convection rolls enhanced mixing conditions and led to larger

droplets along with the rolls than ones away from the rolls.

## 5.1.2 Oiling-out crystallization on micro-structured surfaces

### a. Microlens structures on the surface

A substrate with the polymeric micro-lens array was used in our experiments as shown in Figure 5.8 (a). These micro-lenses could be easily prepared by polymerization of surface droplets, therefore chosen as representative surface micro-structures to reveal the influence of physical structures on oiling-out crystallization. Figure 5.8 b) from  $t_0$  to  $t_0 + 60$  s showed progression of droplet formation where  $t_0$  is defined as a timestamp before observable oiling-out. With micro-lenses on the surface, the number density of droplets is much lower than that on a homogeneous surface, possibly due to fewer nucleation sites on the micro-lenses (Figure 5.7 (d)). The droplets ranged from 5.6  $\mu\text{m}$  to 14.2  $\mu\text{m}$ , much larger than droplets on a homogeneous surface. The effect of the geometric structures on oiling-out droplets appears to be similar to that on the oil droplet formation by solvent exchange[58, 101].

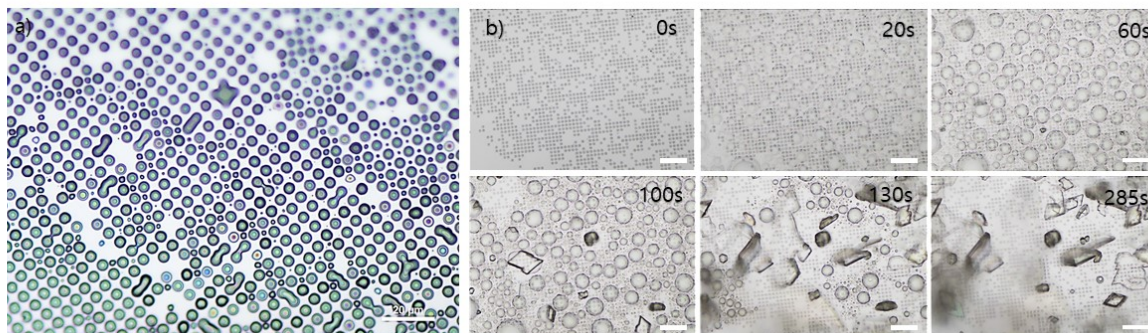


Figure 5.8: Oiling-out crystallization on the lens array. a) an image of the lens array on the substrate b) the snapshot of the solvent exchange process. Length of the scale bar: a) 20  $\mu\text{m}$  and b) 40  $\mu\text{m}$ . Channel height: 300  $\mu\text{m}$ .

More importantly, the micro-lenses have a significant effect on the crystallization process shown in Figure 5.8 (b). The crystals were easily detached from the substrate,

and the crystal shapes were more irregular in comparison to those on the smooth substrates.[26] The easier detachment of crystals may be attributed to the weak adhesion between the crystal plates and the spherical-cap shaped lenses on the substrate. In addition, the lenses caused the crystals to grow in a slightly elevated manner, which also favours crystal detachment. The self-detachment of crystals during the solvent exchange makes it possible for the collection of the crystals from the flow at the exit of the chamber. These collected crystals may be useful as seeds to trigger crystallization in the bulk crystallization[26].

### b. Effects of an inserted bubble

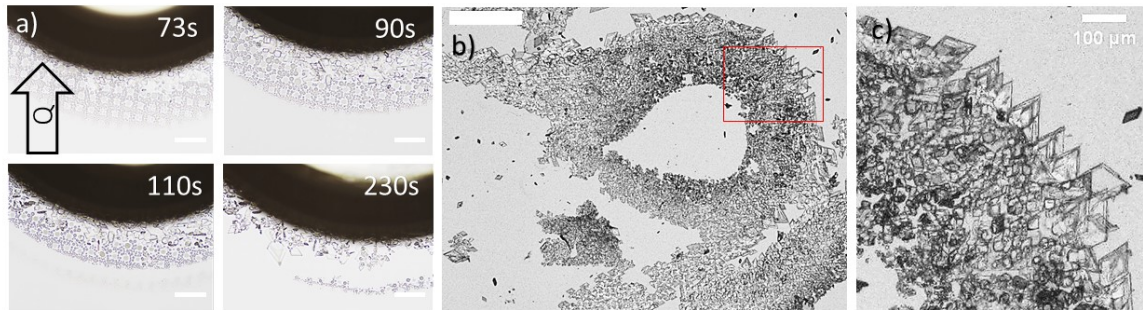


Figure 5.9: a) Oiling-out and crystallization induced by a bubble. The condition for solvent exchange is listed as No. 1 in the Table 3.2. The estimated radius of the bubbles is 1.78 mm. The flow starts from the bottom of the image and flow upward.  $t_0$  is defined as the start of oiling-out. b) Dried alanine crystals on patterned substrate for oiling-out induced by a bubble. The empty circle indicates that bubble used to be there, and the crystallization occurred in the surrounding area. The tail of the crystals that breaks off the circle indicates the direction of the flow. Length of the scale bar: a) and c) 100  $\mu\text{m}$ , b) 500  $\mu\text{m}$

By injection, a small volume of air bubble was inserted into the chamber to mediate the local mixing condition. When a low concentration of 1.5 % alanine were used in solvent exchange system, majority of the surface showed no wide spread droplet formation and crystallization, expect for where the bubble was placed as shown in Figure 5.9. Starting from 110 seconds, second ring of droplets formed due to presence of the bubble. The results suggest that enhanced mixing may be used to form crystals by using a solution with very low alanine concentration. As shown in the enlarged

image of the crystals, the outer edge features more diamond shaped crystals while the inner crystals features bumpy crystals. Such difference in crystal features reflect the difference in local mixing conditions.

The bubble induced crystallization is attributed to the flow rate change and local mixing condition around the bubble. The bubble may act as an obstruction to the main flow and enhance the mixing. As supersaturation rate can be enhanced by the flow rate, more crystallization would be expected when the flow rates are accelerated. The inclusion of a bubble into the solvent exchange system may induce oiling-out crystallization from a lower initial concentration than crystallization methods without bubbles. Meanwhile, we found that the crystallization did not occur for a smaller bubble. Further studies are needed to find preferable bubble size to induce oiling-out crystallization.

### 5.1.3 Fiber crystal formation from droplets without oiling-out

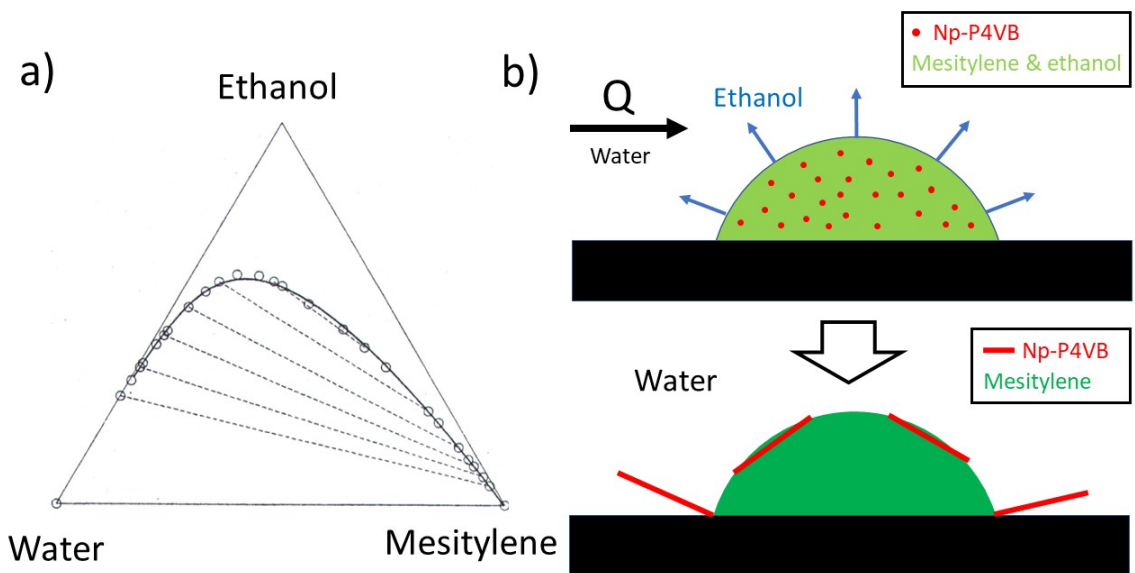


Figure 5.10: a) Ternary phase diagram of mesitylene, water, and ethanol from IUPAC-NIST solubility database[102] b) Sketch of Np-P4VB fiber formation during solvent exchange.

Finally, we will show that the crystal formation by solvent exchange can be applied beyond the oiling-out systems. Np-P4VB was used as the solute for crystallization from droplets consisting of mesitylene, ethanol, and water. The solubility of Np-P4VB is the highest in ethanol and is the lowest in water. During the solvent exchange, solution A contained Np-P4VB, mesitylene, ethanol, and water, and solution B was water as presented in Figure 5.10 (a). Initially, surface droplets were mainly mesitylene with some ethanol and Np-P4VB. As the solvent exchange continued, the droplets became saturated with Np-P4VB as ethanol diffused out into the flow of water and crystallization of Np-P4VB was induced inside the droplets (Figure 5.10 (b)). The crystallization continued until the solute in the droplets was depleted.

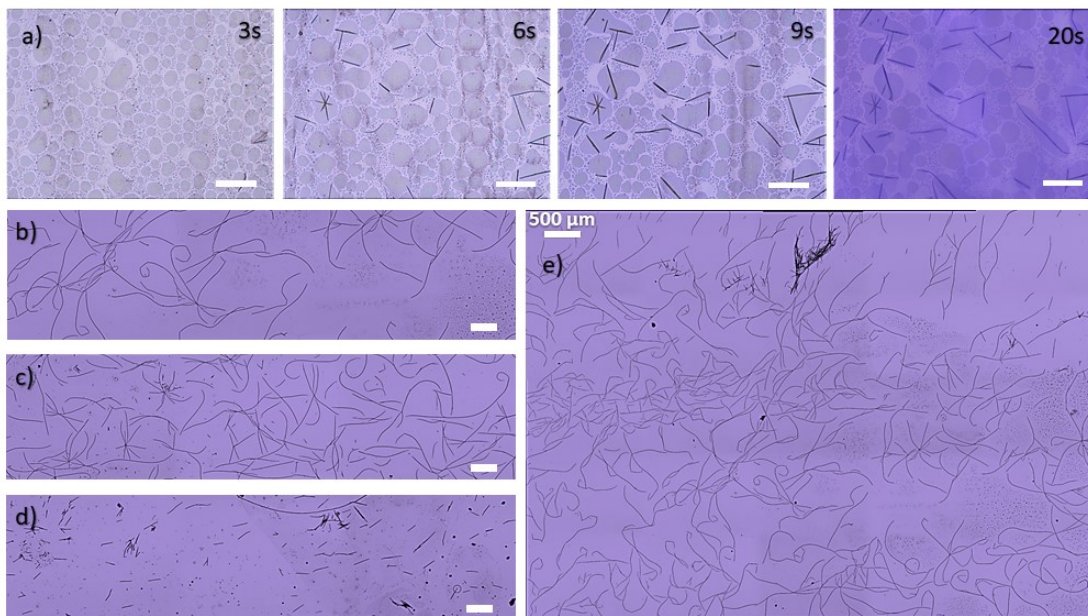


Figure 5.11: Fiber formation in droplet at flow rate of a) 100 mL/hr on OTS substrate through solvent exchange.  $t_0$  is defined as the time when the droplet formation started. Crystal fiber on the substrate after solvent exchange at flow rate of b) 12 mL/hr c) 75 mL/hr d) 100 mL/hr. Length of the scale bar: a) 100  $\mu\text{m}$  b-d) 250  $\mu\text{m}$ . e) Stitched images of crystal fiber formed for b). Total of 25 images were stitched together with 10 % overlapping to manually stitch the images.

The crystal of Np-P4VB formed fibers during the solvent exchange. At a flow rate of 100 mL/hr, the fibers formed inside the droplets and extended with the solvent

exchange process as shown in Figure 5.11 (a). Different from the oiling-out crystallization of alanine, the crystallization initiated from the solute-rich droplets instead of the landed seed crystals, evident from the location of the crystal fibers. The onset of the crystals suggests that supersaturation may be from the reduced ethanol concentration in the droplets during the solvent exchange.

The flow rate affected the crystal fiber formation, and longer fibers were formed at lower flow rates (Figure 5.11 (b)-(d)). For a faster flow rate of 100 mL/hr, there was a significant decrease in fiber length (Figure 5.11 (d)). To capture the bigger picture of the fiber formed on the substrate, the images of the fiber after solvent exchange at 12 mL/hr flow rate have been stitched as a larger image (Figure 5.11 (e)). The results demonstrate that solvent exchange can be applied to control crystallization from droplets containing the solute, not limited to oiling-out systems.

## 5.2 Conclusion

We show that surface micro-patterns can be an effective way to control oiling-out crystallization during solvent exchange. A thin film of crystals can be created with holes on the substrates with hydrophobic micro-patterns. More uniform crystals form on the surfaces with hydrophilic micro-domains, as compared to a homogeneous surfaces. The channel height and flow rate of solvent exchange can be varied to control the oiling-out droplets and crystallization. By using representative micro-structures of polymeric micro-lenses on a substrate, the crystals detached easily from the surface, which may be used for collecting seed crystals to trigger crystallization in the bulk crystallization. Beyond oiling-out systems, solvent exchange can be used to induce crystallization by forming droplets containing the solute that does not exhibit oiling-out behaviour.

The results in the study show great potential in using solvent exchange for crystallization from droplets on the solid surface. Further studies in other chemicals will be valuable for using solvent exchange as a way to control, separate, and purify the

crystal product for pharmaceutical and many other applications.

# Chapter 6

## Conclusions, recommendations, & future work

### 6.1 Conclusions

The experiments with solvent exchange have shown to be effective in controlling the formation of surface droplets and crystallization with oiling-out phenomenon. With adjustment to simple parameters such as flow rate, channel heights, and surface wettability, solvent exchange opens many opportunity for new application in the field of using solvent exchange for crystallization. Various crystal morphology such as polygonal shape, needle-like shape, spherical-cap, or thin film can be achieved on the substrate with good reproducibility. When a patterned substrate was used, further control of the shape of the crystals or even holes in the crystals can be created. By using micro-lenses on the substrate, the crystal detachment was increased which shows potential applications in crystal seed production. In the cases with bubble induced oiling-out crystallization, the limit of initial concentration for crystallization can be further challenged. Lastly, the fiber formation experiment showed that the solvent exchange method is not limited to alanine crystallization but open for other chemicals in the droplets without oiling-out phenomenon. The hope for this study is for the establishment of the link to the oiling-out crystallization studies with the solvent exchange flow cell studies and further develop the work on the combined subjects.

## 6.2 Future work

There are several questions and researches that have not be explored yet in this thesis.

1. The incorporation of other chemicals that exhibit oiling-out crystallization phenomenon with solvent exchange method. While this thesis mainly experimented with beta-alanine, there are still several other chemicals that can experience oiling-out crystallization that may have different crystallization behaviors. Also, many different combinations of solvents and anti-solvents may be used in the future experiments as they have significant effects to the oiling-out crystallization.
2. The other parameters for oiling-out crystallization. As some oiling-out crystallization need different conditions, other parameters such as temperature, PH level, or ultrasound should be explored for oiling-out crystallization through solvent exchange.
3. The bubble induced oiling-out crystallization phenomenon. Clear quantitative connection between the bubble size, initial solute concentration, and the flow rate has not been explored yet. Our current set-up lacked in controlling the bubble size therefore the future experimental apparatus should incorporate a method to do so.
4. Further testing on the patterned substrates. While the patterned substrates have been shown to have effects on droplet nucleation and crystal formation, no study on the effect of different pattern shapes or position have been made. The permeability of the thin film of crystals with holes may be tested for different pattern size and position so that the feasibility for application can be quantified.
5. The tracking of crystal seed development in the flow for solvent exchange. Our current set-up could only track the oiling-out crystallization process on the

substrate therefore the behaviour in the flow was not measured nor captured. By utilizing a PAT, the oiling-out crystallization behaviour may be understood from a micro-fluidics point of view.

# Bibliography

- [1] K. Kiesow, F. Ruether, and G. Sadowski, "Solubility, crystallization and oiling-out behavior of pegdme: 1. pure-solvent systems," *Fluid Phase Equilibria*, vol. 298, pp. 253–261, Nov. 2010. DOI: 10.1016/j.fluid.2010.08.005.
- [2] L. Lafferrère, C. Hoff, and S. Veessler, "Study of liquid–liquid demixing from drug solution," *Journal of Crystal Growth*, vol. 269, pp. 550–557, Sep. 2004. DOI: 10.1016/j.jcrysgro.2004.05.048.
- [3] L. Derdour, "A method to crystallize substances that oil out," *Chemical Engineering Research and Design*, vol. 88, pp. 1174–1181, Sep. 2010. DOI: 10.1016/j.cherd.2010.02.001.
- [4] L. Codan, M. U. Bäbler, and M. Mazzotti, "Phase diagram of a chiral substance exhibiting oiling out in cyclohexane," *Crystal Growth & Design*, vol. 10, pp. 4005–4013, Sep. 2010. DOI: 10.1021/cg100605t.
- [5] M. Takasuga and H. Ooshima, "Control of crystal aspect ratio and size by changing solvent composition in oiling out crystallization of an active pharmaceutical ingredient," *Crystal Growth & Design*, vol. 15, pp. 5834–5838, Nov. 2015. DOI: 10.1021/acs.cgd.5b01192.
- [6] L. Codan, S. Casillo, M. U. Bäbler, and M. Mazzotti, "Phase diagram of a chiral substance exhibiting oiling out. 2. racemic compound forming ibuprofen in water," *Crystal Growth & Design*, vol. 12, pp. 5298–5310, Oct. 2012. DOI: 10.1021/cg300890u.
- [7] X. Li, Q. Yin, M. Zhang, B. Hou, Y. Bao, J. Gong, H. Hao, Y. Wang, J. Wang, and Z. Wang, "Process design for antisolvent crystallization of erythromycin ethylsuccinate in oiling-out system," *Industrial & Engineering Chemistry Research*, vol. 55, pp. 7484–7492, Jul. 2016. DOI: 10.1021/acs.iecr.6b00795.
- [8] J. Lu, Y.-P. Li, J. Wang, Z. Li, S. Rohani, and C.-B. Ching, "Study on the oiling-out and crystallization for the purification of idebenone," *Organic Process Research & Development*, vol. 16, pp. 442–446, Feb. 2012. DOI: 10.1021/op200339a.
- [9] H. Yang and A. C. Rasmuson, "Solubility of butyl paraben in methanol, ethanol, propanol, ethyl acetate, acetone, and acetonitrile," *Journal of Chemical & Engineering Data*, vol. 55, pp. 5091–5093, Nov. 2010. DOI: 10.1021/je1006289.

- [10] H. Yang and A. C. Rasmuson, "Nucleation of butyl paraben in different solvents," *Crystal Growth & Design*, vol. 13, pp. 4226–4238, Sep. 2013. DOI: 10.1021/cg400177u.
- [11] H. Zhao, C. Xie, Z. Xu, Y. Wang, L. Bian, Z. Chen, and H. Hao, "Solution crystallization of vanillin in the presence of a liquid–liquid phase separation," *Industrial & Engineering Chemistry Research*, vol. 51, pp. 14 646–14 652, Oct. 2012. DOI: 10.1021/ie302360u.
- [12] Y. Du, H. Wang, S. Du, Y. Wang, C. Huang, Y. Qin, and J. Gong, "The liquid–liquid phase separation and crystallization of vanillin in 1-propanol/water solution," *Fluid Phase Equilibria*, vol. 409, pp. 84–91, Feb. 2016. DOI: 10.1016/j.fluid.2015.09.011.
- [13] K. Maeda, Y. Nomura, K. Fukui, and S. Hirota, "Separation of fatty acids by crystallization using two liquid phases," *Korean Journal of Chemical Engineering*, vol. 14, pp. 175–178, May 1997. DOI: 10.1007/bf02706091.
- [14] E. Deneau and G. Steele, "An in-line study of oiling out and crystallization," *Organic Process Research & Development*, vol. 9, pp. 943–950, Nov. 2005. DOI: 10.1021/op050107c.
- [15] D. O'Grady, M. Barrett, E. Casey, and B. Glennon, "The effect of mixing on the metastable zone width and nucleation kinetics in the anti-solvent crystallization of benzoic acid," *Chemical Engineering Research and Design*, vol. 85, pp. 945–952, Jan. 2007. DOI: 10.1205/cherd06207.
- [16] T. Tari, P. Szabó-Révész, and Z. Aigner, "Comparative study of different crystallization methods in the case of cilostazol crystal habit optimization," *Crystals*, vol. 9, p. 295, Jun. 2019. DOI: 10.3390/cryst9060295.
- [17] C. Beck, S. V. Dalvi, and R. N. Dave, "Controlled liquid antisolvent precipitation using a rapid mixing device," *Chemical Engineering Science*, vol. 65, pp. 5669–5675, Nov. 2010. DOI: 10.1016/j.ces.2010.04.001.
- [18] J. Kluge, L. Joss, S. Viereck, and M. Mazzotti, "Emulsion crystallization of phenanthrene by supercritical fluid extraction of emulsions," *Chemical Engineering Science*, vol. 77, pp. 249–258, Jul. 2012. DOI: 10.1016/j.ces.2011.12.008.
- [19] K. Pitt, R. Peña, J. D. Tew, K. Pal, R. Smith, Z. K. Nagy, and J. D. Lister, "Particle design via spherical agglomeration: A critical review of controlling parameters, rate processes and modelling," *Powder Technology*, vol. 326, pp. 327–343, Feb. 2018. DOI: 10.1016/j.powtec.2017.11.052.
- [20] Y. Kawashima, M. Okumura, and H. Takenaka, "Spherical crystallization: Direct spherical agglomeration of salicylic acid crystals during crystallization," *Science*, vol. 216, pp. 1127–1128, Jun. 1982. DOI: 10.1126/science.216.4550.1127.

- [21] M. Sun, S. Du, M. Chen, S. Rohani, H. Zhang, Y. Liu, P. Sun, Y. Wang, P. Shi, S. Xu, and J. Gong, "Oiling-out investigation and morphology control of  $\beta$ -alanine based on ternary phase diagrams," *Crystal Growth & Design*, vol. 18, pp. 818–826, Jan. 2018. DOI: 10.1021/acs.cgd.7b01293.
- [22] H. Yang, M. Svård, J. Zeglinski, and A. C. Rasmuson, "Influence of solvent and solid-state structure on nucleation of parabens," *Crystal Growth & Design*, vol. 14, pp. 3890–3902, Jul. 2014. DOI: 10.1021/cg500449d.
- [23] M. Sun, W. Tang, S. Du, Y. Zhang, X. Fu, and J. Gong, "Understanding the roles of oiling-out on crystallization of  $\beta$ -alanine: Unusual behavior in metastable zone width and surface nucleation during growth stage," *Crystal Growth & Design*, vol. 18, pp. 6885–6890, Oct. 2018. DOI: 10.1021/acs.cgd.8b01096.
- [24] H. Yang, H. Chen, and A. C. Rasmuson, "Sandwich crystals of butyl paraben," *CrystEngComm*, vol. 16, pp. 8863–8873, 2014. DOI: 10.1039/c4ce01320d.
- [25] K. Li, S. Wu, S. Xu, S. Du, K. Zhao, L. Lin, P. Yang, B. Yu, B. Hou, and J. Gong, "Oiling out and polymorphism control of pyraclostrobin in cooling crystallization," *Industrial & Engineering Chemistry Research*, vol. 55, pp. 11 631–11 637, Oct. 2016. DOI: 10.1021/acs.iecr.6b03097.
- [26] X. Zhang, Z. Wei, H. Choi, H. Hao, and H. Yang, "Oiling-out crystallization of beta-alanine on solid surfaces controlled by solvent exchange," *Advanced Materials Interfaces*, p. 2001 200, Oct. 2020. DOI: 10.1002/admi.202001200.
- [27] J. Lu, K. Carpenter, R.-J. Li, X.-J. Wang, and C.-B. Ching, "Cloud-point temperature and liquid–liquid phase separation of supersaturated lysozyme solution," *Biophysical Chemistry*, vol. 109, pp. 105–112, Apr. 2004. DOI: 10.1016/j.bpc.2003.10.021.
- [28] D. Lohse and X. Zhang, "Surface nanobubbles and nanodroplets," *Reviews of Modern Physics*, vol. 87, pp. 981–1035, Aug. 2015. DOI: 10.1103/revmodphys.87.981.
- [29] X. H. Zhang and W. Ducker, "Formation of interfacial nanodroplets through changes in solvent quality," *Langmuir*, vol. 23, pp. 12 478–12 480, Dec. 2007. DOI: 10.1021/la702453g.
- [30] X. Zhang, Z. Lu, H. Tan, L. Bao, Y. He, C. Sun, and D. Lohse, "Formation of surface nanodroplets under controlled flow conditions," *Proceedings of the National Academy of Sciences*, vol. 112, pp. 9253–9257, Jul. 2015. DOI: 10.1073/pnas.1506071112.
- [31] M. Li, L. Bao, H. Yu, and X. Zhang, "Formation of multicomponent surface nanodroplets by solvent exchange," *The Journal of Physical Chemistry C*, vol. 122, pp. 8647–8654, Mar. 2018. DOI: 10.1021/acs.jpcc.8b01448.
- [32] B. Dyett, A. Kiyama, M. Rump, Y. Tagawa, D. Lohse, and X. Zhang, "Growth dynamics of surface nanodroplets during solvent exchange at varying flow rates," *Soft Matter*, vol. 14, pp. 5197–5204, 2018. DOI: 10.1039/c8sm00705e.

- [33] B. Dyett, H. Yu, and X. Zhang, “Formation of surface nanodroplets of viscous liquids by solvent exchange,” *The European Physical Journal E*, vol. 40, Mar. 2017. DOI: 10.1140/epje/i2017-11514-8.
- [34] J. Meng, J. B. You, and X. Zhang, “Viscosity-mediated growth and coalescence of surface nanodroplets,” *The Journal of Physical Chemistry C*, vol. 124, pp. 12 476–12 484, May 2020. DOI: 10.1021/acs.jpcc.0c02220.
- [35] X. Zhang, J. Ren, H. Yang, Y. He, J. Tan, and G. G. Qiao, “From transient nanodroplets to permanent nanolenses,” *Soft Matter*, vol. 8, p. 4314, 2012. DOI: 10.1039/c2sm07267j.
- [36] Z. Lu, H. Xu, H. Zeng, and X. Zhang, “Solvent effects on the formation of surface nanodroplets by solvent exchange,” *Langmuir*, vol. 31, pp. 12 120–12 125, Oct. 2015. DOI: 10.1021/acs.langmuir.5b03303.
- [37] J. Qian, G. F. Arends, and X. Zhang, “Surface nanodroplets: Formation, dissolution, and applications,” *Langmuir*, vol. 35, pp. 12 583–12 596, May 2019. DOI: 10.1021/acs.langmuir.9b01051.
- [38] H. Xu and X. Zhang, “Formation, characterization and stability of oil nanodroplets on immersed substrates,” *Advances in Colloid and Interface Science*, vol. 224, pp. 17–32, Oct. 2015. DOI: 10.1016/j.cis.2015.07.004.
- [39] M. Li, R. Cao, B. Dyett, and X. Zhang, “Encapsulated nanodroplets for enhanced fluorescence detection by nano-extraction,” *Small*, vol. 16, p. 2 004 162, Oct. 2020. DOI: 10.1002/smll.202004162.
- [40] S. Peng and X. Zhang, “Simple nanodroplet templating of functional surfaces with tailored wettability and microstructures,” *Chemistry - An Asian Journal*, vol. 12, pp. 1538–1544, May 2017. DOI: 10.1002/asia.201700358.
- [41] J. Hou, H. Zhang, Q. Yang, M. Li, Y. Song, and L. Jiang, “Bio-inspired photonic-crystal microchip for fluorescent ultratrace detection,” *Angewandte Chemie*, vol. 126, pp. 5901–5905, Mar. 2014. DOI: 10.1002/ange.201400686.
- [42] Y. Zhu and Q. Fang, “Analytical detection techniques for droplet microfluidics—a review,” *Analytica Chimica Acta*, vol. 787, pp. 24–35, Jul. 2013. DOI: 10.1016/j.aca.2013.04.064.
- [43] W. Qiao, T. Zhang, T. Yen, T.-H. Ku, J. Song, I. Lian, and Y.-H. Lo, “Oil-encapsulated nanodroplet array for bio-molecular detection,” *Annals of Biomedical Engineering*, vol. 42, pp. 1932–1941, May 2014. DOI: 10.1007/s10439-014-1039-z.
- [44] S. A. Vitale and J. L. Katz, “Liquid droplet dispersions formed by homogeneous liquidliquid nucleation: “the ouzo effect”,” *Langmuir*, vol. 19, pp. 4105–4110, May 2003. DOI: 10.1021/la026842o.
- [45] S. Alberti, A. Gladfelter, and T. Mittag, “Considerations and challenges in studying liquid-liquid phase separation and biomolecular condensates,” *Cell*, vol. 176, pp. 419–434, Jan. 2019. DOI: 10.1016/j.cell.2018.12.035.

- [46] L. Bao, A. R. Rezk, L. Y. Yeo, and X. Zhang, “Highly ordered arrays of femtoliter surface droplets,” *Small*, vol. 11, pp. 4850–4855, Jul. 2015. DOI: 10.1002/sml.201501105.
- [47] Z. Lu, S. Peng, and X. Zhang, “Influence of solution composition on the formation of surface nanodroplets by solvent exchange,” *Langmuir*, vol. 32, pp. 1700–1706, Feb. 2016. DOI: 10.1021/acs.langmuir.5b04630.
- [48] M. Guan, W. Guo, L. Gao, Y. Tang, J. Hu, and Y. Dong, “Investigation on the temperature difference method for producing nanobubbles and their physical properties,” *ChemPhysChem*, vol. 13, pp. 2115–2118, Apr. 2012. DOI: 10.1002/cphc.201100912.
- [49] H. Yu, Z. Lu, D. Lohse, and X. Zhang, “Gravitational effect on the formation of surface nanodroplets,” *Langmuir*, vol. 31, pp. 12 628–12 634, Nov. 2015. DOI: 10.1021/acs.langmuir.5b03464.
- [50] Z. Lu, M. H. Klein, X. Zhu, L. Y. Yeo, D. Lohse, and X. Zhang, “Universal nanodroplet branches from confining the ouzo effect,” *Proceedings of the National Academy of Sciences*, vol. 114, pp. 10 332–10 337, Sep. 2017. DOI: 10.1073/pnas.1704727114.
- [51] H. Yu, S. Maheshwari, J. Zhu, D. Lohse, and X. Zhang, “Formation of surface nanodroplets facing a structured microchannel wall,” *Lab on a Chip*, vol. 17, pp. 1496–1504, 2017. DOI: 10.1039/c6lc01555g.
- [52] B. Zeng, Y. Wang, X. Zhang, and D. Lohse, “Solvent exchange in a hele–shaw cell: Universality of surface nanodroplet nucleation,” *The Journal of Physical Chemistry C*, vol. 123, pp. 5571–5577, Feb. 2019. DOI: 10.1021/acs.jpcc.9b00298.
- [53] H. Yu, S. Peng, L. Lei, J. Zhang, T. L. Greaves, and X. Zhang, “Large scale flow-mediated formation and potential applications of surface nanodroplets,” *ACS Applied Materials & Interfaces*, vol. 8, pp. 22 679–22 687, Aug. 2016. DOI: 10.1021/acsami.6b07200.
- [54] H. Yu, M. Rump, S. Maheshwari, L. Bao, and X. Zhang, “Growth of nanodroplets on a still microfiber under flow conditions,” *Physical Chemistry Chemical Physics*, vol. 20, pp. 18 252–18 261, 2018. DOI: 10.1039/c8cp02353k.
- [55] P.-G. D. Gennes, F. Brochard-Wyart, and D. Quere, *Capillarity and Wetting Phenomena : Drops, Bubbles, Pearls, Waves*. Springer, 2010.
- [56] X. Zhang, J. Wang, L. Bao, E. Dietrich, R. C. A. van der Veen, S. Peng, J. Friend, H. J. W. Zandvliet, L. Yeo, and D. Lohse, “Mixed mode of dissolving immersed nanodroplets at a solid–water interface,” *Soft Matter*, vol. 11, pp. 1889–1900, 2015. DOI: 10.1039/c4sm02397h.
- [57] S. Peng, D. Lohse, and X. Zhang, “Spontaneous pattern formation of surface nanodroplets from competitive growth,” *ACS Nano*, vol. 9, pp. 11 916–11 923, Nov. 2015. DOI: 10.1021/acs.nano.5b04436.

- [58] S. Peng, I. Dević, H. Tan, D. Lohse, and X. Zhang, “How a surface nanodroplet sits on the rim of a microcap,” *Langmuir*, vol. 32, pp. 5744–5754, Jun. 2016. DOI: 10.1021/acs.langmuir.6b01153.
- [59] S. Peng, B.-E. Pinchasik, H. Hao, H. Möhwald, and X. Zhang, “Morphological transformation of surface femtodroplets upon dissolution,” *The Journal of Physical Chemistry Letters*, vol. 8, pp. 584–590, Jan. 2017. DOI: 10.1021/acs.jpcllett.6b02861.
- [60] L. Bao, B.-E. Pinchasik, L. Lei, Q. Xu, H. Hao, X. Wang, and X. Zhang, “Control of femtoliter liquid on a microlens: A way to flexible dual-microlens arrays,” *ACS Applied Materials & Interfaces*, vol. 11, pp. 27 386–27 393, Jul. 2019. DOI: 10.1021/acsami.9b06390.
- [61] T. E. Faber, *Fluid Dynamics for Physicists*. Cambridge University Press, 1995.
- [62] M. Li, B. Dyett, H. Yu, V. Bansal, and X. Zhang, “Functional femtoliter droplets for ultrafast nanoextraction and supersensitive online microanalysis,” *Small*, vol. 15, p. 1 804 683, Nov. 2018. DOI: 10.1002/sml.201804683. (visited on 11/26/2020).
- [63] M. Li, H. Yu, L. Bao, B. Dyett, and X. Zhang, “Controlled addition of new liquid component into surface droplet arrays by solvent exchange,” *Journal of Colloid and Interface Science*, vol. 543, pp. 164–173, May 2019. DOI: 10.1016/j.jcis.2019.02.046.
- [64] L. Lei, J. Li, H. Yu, L. Bao, S. Peng, and X. Zhang, “Formation, growth and applications of femtoliter droplets on a microlens,” *Physical Chemistry Chemical Physics*, vol. 20, pp. 4226–4237, 2018. DOI: 10.1039/c7cp06861a.
- [65] L. Malic, T. Veres, and M. Tabrizian, “Two-dimensional droplet-based surface plasmon resonance imaging using electrowetting-on-dielectric microfluidics,” *Lab Chip*, vol. 9, pp. 473–475, 2009. DOI: 10.1039/b814697g. (visited on 02/16/2021).
- [66] C. H. Jeong, H. J. Lee, D. Y. Kim, S. B. Ahangar, C. K. Choi, and S. H. Lee, “Quantitative analysis of contact line behaviors of evaporating binary mixture droplets using surface plasmon resonance imaging,” *International Journal of Heat and Mass Transfer*, vol. 165, p. 120 690, Feb. 2021. DOI: 10.1016/j.ijheatmasstransfer.2020.120690. (visited on 02/16/2021).
- [67] D. C. Ash, M. J. Joyce, C. Barnes, C. J. Booth, and A. C. Jefferies, “Viscosity measurement of industrial oils using the droplet quartz crystal microbalance,” *Measurement Science and Technology*, vol. 14, pp. 1955–1962, Sep. 2003. DOI: 10.1088/0957-0233/14/11/013.
- [68] N. T. Pham, G. McHale, M. I. Newton, B. J. Carroll, and S. M. Rowan, “Application of the quartz crystal microbalance to the evaporation of colloidal suspension droplets,” *Langmuir*, vol. 20, pp. 841–847, Feb. 2004. DOI: 10.1021/la0357007. (visited on 02/16/2021).
- [69] J. W. Mullin, *Crystallization*. Butterworth-Heinemann, 2001.

- [70] A. Mersmann, *Crystallization Technology Handbook*. Marcel Dekker, 2001.
- [71] I. de Albuquerque and M. Mazzotti, “Crystallization process design using thermodynamics to avoid oiling out in a mixture of vanillin and water,” *Crystal Growth & Design*, vol. 14, pp. 5617–5625, Sep. 2014. DOI: 10.1021/cg500904v.
- [72] C. C. Sun, “Cocrystallization for successful drug delivery,” *Expert Opinion on Drug Delivery*, vol. 10, pp. 201–213, Dec. 2012. DOI: 10.1517/17425247.2013.747508.
- [73] A. S. Myerson, D. Erdemir, and A. Y. Lee, *Handbook of Industrial Crystallization*. Cambridge, United Kingdom ; New York, Ny Cambridge University Press, 2019.
- [74] A. T. M. Serajudin and M. Pudipeddi, *Salt selection strategies, in Handbook of Pharmaceutical Salts: Properties, Selection And Use*, Stahl, P.H. and Wermuth, C.G., Wermuth, C.G. VHCA, Verlag Helvetica Chimica Acta/Wiley-VCH, Zürich/Weinheim, 2002, pp. 135 –160.
- [75] W. Beckmann, “Seeding the desired polymorph: Background, possibilities, limitations, and case studies,” *Organic Process Research & Development*, vol. 4, pp. 372–383, Sep. 2000. DOI: 10.1021/op0000778.
- [76] Z. Meng, Y. Huang, S. Cheng, and J. Wang, “Investigation of oiling-out phenomenon of small organic molecules in crystallization processes: A review,” *ChemistrySelect*, vol. 5, pp. 7855–7866, Jul. 2020. DOI: 10.1002/slct.202001255.
- [77] Z. Q. Yu, P. S. Chow, and R., “Application of attenuated total reflectance fourier transform infrared technique in the monitoring and control of anti-solvent crystallization,” *Industrial & Engineering Chemistry Research*, vol. 45, pp. 438–444, Jan. 2006. DOI: 10.1021/ie050660i.
- [78] K. Sangwal, *Nucleation and Crystal Growth Metastability of Solutions and Melts*. Hoboken, Nj John Wiley & Sons, 2018.
- [79] P. G. Vekilov, “Nucleation,” *Crystal Growth & Design*, vol. 10, pp. 5007–5019, Dec. 2010. DOI: 10.1021/cg1011633.
- [80] H. Yang, “Relation between metastable zone width and induction time of butyl paraben in ethanol,” *Royal society of chemistry*, vol. 17, p. 577, 2015. DOI: 10.1039/c4ce01625d.
- [81] K. Maeda, Y. Aoyama, K. Fukui, and S. Hirota, “Novel phenomena of crystallization and emulsification of hydrophobic solute in aqueous solution,” *Journal of Colloid and Interface Science*, vol. 234, pp. 217–222, Feb. 2001. DOI: 10.1006/jcis.2000.7316.
- [82] C. Li, J. Huang, and Z. Li, “A relation for nanodroplet diffusion on smooth surfaces,” *Scientific Reports*, vol. 6, May 2016. DOI: 10.1038/srep26488.
- [83] S. Veessler, E. Revalor, O. Bottini, and C. Hoff, “Crystallization in the presence of a liquidliquid phase separation,” *Organic Process Research & Development*, vol. 10, pp. 841–845, Jul. 2006. DOI: 10.1021/op060085+.

- [84] S. Daver, N. Rodeville, F. Pineau, J.-M. Arlabosse, C. Moureou, F. Muller, R. Pierre, K. Bouquet, L. Dumais, J.-G. Boiteau, and I. Cardinaud, "Process development and crystallization in oiling-out system of a novel topical antian-drogen," *Organic Process Research & Development*, vol. 21, pp. 231–240, Jan. 2017. DOI: 10.1021/acs.oprd.6b00392.
- [85] P. E. Bonnett, K. J. Carpenter, S. Dawson, and R. J. Davey, "Solution crys-tallisation via a submerged liquid–liquid phase boundary: Oiling out," *Chem-ical Communications*, pp. 698–699, Feb. 2003. DOI: 10.1039/b212062c.
- [86] S. Kim, C. Wei, and S. Kiang, "Crystallization process development of an active pharmaceutical ingredient and particle engineering via the use of ultra-sonics and temperature cycling," *Organic Process Research & Development*, vol. 7, pp. 997–1001, Nov. 2003. DOI: 10.1021/op034107t.
- [87] K. Kiesow, F. Tumakaka, and G. Sadowski, "Experimental investigation and prediction of oiling out during crystallization process," *Journal of Crystal Growth*, vol. 310, pp. 4163–4168, Aug. 2008. DOI: 10.1016/j.jcrysgro.2008.06.034. [Online]. Available: <https://www.sciencedirect.com/science/article/pii/S0022024808004910>.
- [88] R. Ren, D. Sun, T. Wei, S. Zhang, and J. Gong, "The role of diastereomer impurity in oiling-out during the resolution of trans-4-methyl-2-piperidine carboxylic ethyl ester enantiomers by crystallization," *Organic Process Research & Development*, vol. 18, pp. 709–716, May 2014. DOI: 10.1021/op500026z.
- [89] Z. Gao, F. Altimimi, J. Gong, Y. Bao, J. Wang, and S. Rohani, "Ultrasonic irradiation and seeding to prevent metastable liquid–liquid phase separation and intensify crystallization," *Crystal Growth & Design*, vol. 18, pp. 2628–2635, Mar. 2018. DOI: 10.1021/acs.cgd.8b00284.
- [90] P. Parimaladevi, S. Supriya, and K. Srinivasan, "The role of ultrasound in controlling the liquid-liquid phase separation and nucleation of vanillin poly-morphs i and ii," *Journal of Crystal Growth*, vol. 484, pp. 21–30, Feb. 2018. DOI: 10.1016/j.jcrysgro.2017.12.023.
- [91] H. Yang and A. C. Rasmuson, "Investigation of batch cooling crystallization in a liquid–liquid separating system by pat," *Organic Process Research & De-velopment*, vol. 16, pp. 1212–1224, Jun. 2012. DOI: 10.1021/op200355b.
- [92] P. G. Vekilov, "Dense liquid precursor for the nucleation of ordered solid phases from solution," *Crystal Growth & Design*, vol. 4, pp. 671–685, Jul. 2004. DOI: 10.1021/cg049977w.
- [93] R. J. Davey, S. L. M. Schroeder, and J. H. terHorst, "Nucleation of organic crystals-a molecular perspective," *Angewandte Chemie International Edition*, vol. 52, pp. 2166–2179, Jan. 2013. DOI: 10.1002/anie.201204824.
- [94] D. Gebauer, M. Kellermeier, J. D. Gale, L. Bergström, and H. Cölfen, "Pre-nucleation clusters as solute precursors in crystallisation," *Chem. Soc. Rev.*, vol. 43, pp. 2348–2371, 2014. DOI: 10.1039/c3cs60451a.

- [95] Y. Kawashima, T. Niwa, T. Handa, H. Takeuchi, T. Iwamoto, and K. Itoh, "Preparation of controlled-release microspheres of ibuprofen with acrylic polymers by a novel quasi-emulsion solvent diffusion method," *Journal of Pharmaceutical Sciences*, vol. 78, pp. 68–72, Jan. 1989. DOI: 10.1002/jps.2600780118.
- [96] M. Nocent, L. Bertocchi, F. Espitalier, M. Baron, and G. Couarraze, "Definition of a solvent system for spherical crystallization of salbutamol sulfate by quasi-emulsion solvent diffusion (quesd) method," *Journal of Pharmaceutical Sciences*, vol. 90, pp. 1620–1627, Oct. 2001. DOI: 10.1002/jps.1112.
- [97] X. H. Zhang, A. Quinn, and W. A. Ducker, "Nanobubbles at the interface between water and a hydrophobic solid," *Langmuir*, vol. 24, pp. 4756–4764, May 2008. DOI: 10.1021/la703475q.
- [98] S. Lane, S. Vagin, H. Wang, W. R. Heinz, W. Morrish, Y. Zhao, B. Rieger, and A. Meldrum, "Wide-gamut lasing from a single organic chromophore," *Light: Science & Applications*, vol. 7, Dec. 2018. DOI: 10.1038/s41377-018-0102-1.
- [99] S. Abramov, P. Ruppik, and H. Schuchmann, "Crystallization in emulsions: A thermo-optical method to determine single crystallization events in droplet clusters," *Processes*, vol. 4, p. 25, Aug. 2016. DOI: 10.3390/pr4030025.
- [100] D. Shanthi, P. Selvarajan, K. HemaDurga, and S. Lincy Mary Ponmani, "Nucleation kinetics, growth and studies of  $\beta$ -alanine single crystals," *Spectrochimica Acta Part A: Molecular and Biomolecular Spectroscopy*, vol. 110, pp. 1–6, Jun. 2013. DOI: 10.1016/j.saa.2013.02.040.
- [101] B. Dyett, H. Hao, D. Lohse, and X. Zhang, "Coalescence driven self-organization of growing nanodroplets around a microcap," *Soft Matter*, vol. 14, pp. 2628–2637, 2018. DOI: 10.1039/c7sm02490h.
- [102] A Skrzecz, *Solubility system: Ethanol with mesitylene (1,3,5-trimethylbenzene) and water*, IUPAC-NIST Solubility Database NIST Standard Reference Database 106, May 1997. [Online]. Available: [https://srdata.nist.gov/solubility/sol\\_detail.aspx?sysID=69\\_120](https://srdata.nist.gov/solubility/sol_detail.aspx?sysID=69_120).

# Appendix A:

## A.1 Section 1

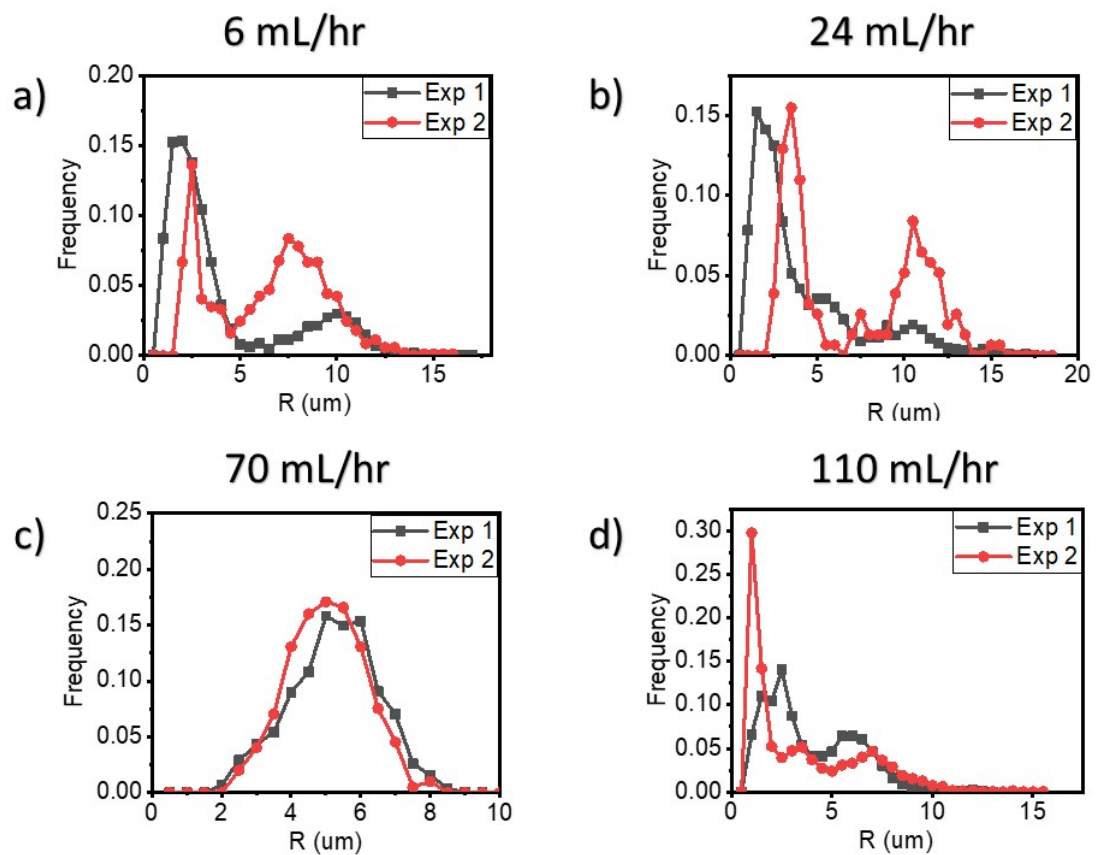


Figure A.1: Plot of droplet size distribution on  $SiO_2$  before crystals were observed in the view of the microscope. Flow rate of a) 6 mL/hr, b) 24 mL/hr, c) 70 mL/hr, and d) 110 mL/hr.